

This document is confidential and is proprietary to the American Chemical Society and its authors. Do not copy or disclose without written permission. If you have received this item in error, notify the sender and delete all copies.

**Regular Solution Theory for Polymer Permeation Transients:
A Toolkit for Understanding Experimental Waveshapes**

Journal:	<i>Langmuir</i>
Manuscript ID	Draft
Manuscript Type:	Article
Date Submitted by the Author:	n/a
Complete List of Authors:	Craster, Bernadette; TWI Wadhawan, Jay; University of Hull, Department of Physical Sciences (Chemistry) Lawrence, Nathan; University of Hull, Kelly, Stephen; University of Hull, Organic and Materials Chemistry, Department of Chemistry

SCHOLARONE™
Manuscripts

This document is the Accepted Manuscript version of a Published Work that appeared in final form in Langmuir, copyright © American Chemical Society after peer review and technical editing by the publisher. To access the final edited and published work see: [10.1021/acs.langmuir.0c00589](https://doi.org/10.1021/acs.langmuir.0c00589)

1
2
3 **Regular Solution Theory for Polymer Permeation Transients:**
4 **A Toolkit for Understanding Experimental Waveshapes**
5
6

7 Jay D. Wadhawan,^{1,2*} Bernadette Craster,^{3*} Nathan S. Lawrence,^{1,2} Stephen M. Kelly.^{2,4}
8
9

10 ¹*Department of Chemical Engineering, The University of Hull,*
11 *Cottingham Road, Kingston-upon-Hull HU6 7RX, United Kingdom.*
12

13
14 ²*Aura Innovation Centre, Bridgehead Business Park,*
15 *Meadow Road, Hessle HU13 0GD, United Kingdom.*
16

17
18 ³*TWI, Ltd., Bevan Braithwaite Building, Granta Park,*
19 *Great Abington, Cambridge CB21 6AL, United Kingdom.*
20

21
22
23 ⁴*Department of Chemistry and Biochemistry, The University of Hull,*
24 *Cottingham Road, Kingston-upon-Hull HU6 7RX, United Kingdom.*
25
26
27
28
29
30
31
32
33
34
35
36
37
38
39
40
41
42
43
44
45
46
47
48
49
50
51
52
53
54

55 To be submitted to *Langmuir*
56

57
58 *Corresponding authors
59

60 E.mail: j.wadhawan@hull.ac.uk (JDW); bernadette.craster@twi.co.uk (BC)

Abstract

The accurate measurement of permeation is important at the product design stage for a variety of industries as diverse as conveyancing methods for oil and gas produced fluids, such as mixtures of carbon dioxide, methane, hydrogen sulfide, water and hydrocarbons, in polymer-lined, unbonded flexible risers and flow lines through connectors and valves; hydrogen and methane gas carrying domestic lines; hydrogen storage tanks; sulfur hexafluoride circuit breakers for high power-carrying lines; oxygen through display technology; and drug delivery. It would also be appropriate to monitor the permeation rate through the polymer, composite and elastomeric layers during the in-service times where applications allow. In the future, any alteration in the short term and long term transport rates could be analysed in terms of an initial alteration or degradation of the polymeric materials, and in some cases, metallic components. Crucially, such measurements would serve as an early warning system of any change in a polymeric material that could result in loss of function as fluid of gas containing barrier material.

Most experimental determinations are made through recording flux transients (varying flux) through permeation cells in which a polymer membrane or film separates a donor compartment (usually an infinite supply) and an acceptor compartment, and in which membrane transport is considered as slow. Treatment of the resulting experimental data is usually, but not always, undertaken through comparison with a steady-state model based on Fickian diffusion through the membrane, so as to extract the membrane permeability, the diffusion coefficient of the permeant and the solubility of the permeant in the membrane phase. However, in spite of these measurements being undertaken routinely using closed cell manometric or continuous flow methods, there is a lack of literature in which experimental flux transients are provided, and in several cases, it is clear that the experimental data do not conform to the expected model of slow, Fickian diffusion through the membrane, even though experiments are performed at temperatures much larger than the glass transition temperature of the polymer membrane.

In this paper, we first re-examine the classical model for an infinite source, and extend it to account for (1) molecular interactions between membrane and permeant, using regular solution theory, (2) slow transport in the acceptor phase, and (3) slow kinetics across the membrane | acceptor interface. We demonstrate that all three aspects can cause permeation flux transients to exhibit unusual, non-classical waveshapes, which have nevertheless been experimentally realized without rationalization. This enables the development of an algorithmic toolkit for the interpretation of permeation flux transients, so as to provide reliable and accurate data analysis for experimentalists.

Key words: Permeation, flux transient, non-Fickian diffusion, regular solutions, interfacial kinetics, membranes, finite-difference simulation, polymer membrane, continuous flow, closed cell manometric.

Introduction

The movement of chemical species from a source (donor) to a sink (receptor or acceptor) through a permeable material (such as a membrane) is extremely important, and finds applications in a huge diversity of fields.¹ For the oil and gas industry, examples are in various flow line configurations where the fluid containment, and in some instances, the protection of metallic components from degradation through corrosion, can reduce the risk of accidental leakage of oil and gas into the local environment on land or at sea.²⁻⁴ In fact, the accurate measurement of permeation is important at the product design stage for a variety of industries as diverse as conveyancing methods for oil and gas produced fluids, such as mixtures of carbon dioxide, methane, hydrogen sulfide, water and hydrocarbons, in polymer-lined carbon steel pipes;⁵ unbonded flexible risers and flow lines through connectors and valves; hydrogen and methane gas carrying domestic lines;⁶ hydrogen storage tanks;⁷ sulfur hexafluoride circuit breakers for high power-carrying lines;⁸ oxygen through display technology; and in the exclusion of toxic chemicals by suitable chemical safety clothing, and in the delivery of important pharmaceutical drugs across biological membranes such as the skin.⁹ It would also be appropriate to monitor the permeation rate through the polymer, composite and elastomeric layers during the in-service times, where applications allow. In the future, any alteration in the short term and long term transport rates could be analysed in terms of an initial alteration or degradation of the polymeric materials, and in some cases, metallic components. Crucially, such measurements would serve as an early warning system of any change in a polymeric material that could result in loss of function as fluid of gas containing barrier material. Other instances are in fuel cell and industrial electrolyser design, where membranes or porous ceramics separate anolyte and catholyte;¹⁰ in pharmaceutical science, where it is important to characterise the dose dependency of medical drugs for percutaneous absorption;¹¹ and in environmental engineering, where groundwater quality is influenced by mineral permeation through soil and geological stratigraphic layers.¹² Furthermore, in the chemical industry, permeation is important for a number of separation processes.^{13,14}

Experimentally, transport through membranes is quantified in one of three ways:¹⁵ (1) studies involving sorption-desorption process in which a negligibly thick polymer film is immersed into a permeant solution, and the mass increase in the polymer film is recorded; (2) membrane permeation at constant volume where the permeant diffuses from a donor compartment to a receiver cell of constant volume, where it is detected; or (3) constant pressure permeation through a membrane into a flowing stream, where it is detected. Normally the experiment type as described in (2) above, is carried out as a closed-cell manometric method and is ideal for single component species.¹⁶ Usually these experiments are run for a few hours. The experiment in type (3) is often called the continuous flow method and is suited for studying the permeation of mixtures. These latter experiments can be run for several weeks with the concentrations monitored using mass spectrometry or gas chromatography. Such experiments have led to extensive literature pertaining to the

1
2
3 molecular mechanisms underpinning permeation,¹⁷ based on a diffusion model with attention
4 paid to both the chemical affinity of the diffusing species to the membrane,¹⁸ and to the effect
5 of the donor delivery solvent on the diffusivity of the permeant.¹⁹ For polymeric membranes
6 at temperatures above the glass transition temperature, the rotational motion of the polymer
7 chains enables the structure to respond rapidly to changes in its conditions.²⁰ *Accordingly,*
8 *equilibrium is considered to be established rapidly when a fluid contacts a polymer*
9 *membrane, so that, in a variety of theoretical models, it is assumed that the rate-limiting*
10 *step in the permeation process is analyte diffusion across the membrane.*²¹ This encourages
11 experimental results to be analysed when the system approaches a *steady state*, from which
12 the permeability coefficient (a product of the permeant diffusion coefficient and species
13 solubility) may be estimated.²² Indeed, at steady-state, Fickian diffusion of the permeant in
14 the membrane yields proportionality of the quantity of diffusing material across the
15 membrane with time (*vide infra*), so that the “time lag” to steady-state affords the (constant)
16 permeant diffusion coefficient.²³

24 To account for the non-Fickian behaviour that is often observed for transport through
25 polymers in the glassy state, Frisch²⁴ categorised the transport of small molecules through
26 polymers, based on the time-dependent mass uptake of a polymer film through the ratio,

27
28
29
$$\frac{M_t}{M_\infty} \propto t^n$$

30 any time, t, compared with that obtained in the limit of steady-state (M_∞), with the exponent n
31 distinguishing the diffusion mechanism. The classical case of Fickian diffusion (Case 1) has
32 n = 1/2, signifying the rate of diffusion being less than the characteristic relaxation time of the
33 polymer motions, and where membrane swelling due to the permeant is insignificant. This
34 type of behaviour is, as indicated above, often observed whenever the polymer temperature is
35 *very much greater* than its glass transition temperature (T_g).²⁵ When $1/2 \leq n < 1$, anomalous
36 diffusion (“dual sorption mechanism”) occurs, since the rate at which penetrant diffusion
37 occurs is comparable with the polymer relaxation rate. This can only occur when the
38 experimental temperature is *lower* than the glass transition temperature, since polymer chain
39 motion is not sufficiently rapid to homogenise the environment around the permeant,²⁶ and
40 in some polymers, the permeability is pressure-dependent above T_g . Under these conditions,
41 it is assumed that two mechanisms operate: the first is the diffusion of the *absorbed*
42 permeant, and the second is the occurrence of *strongly adsorbed* permeant molecules which
43 are essentially considered immobile and so do not participate in the diffusion process.²⁷ If the
44 permeant diffusion rate becomes more rapid than the polymer relaxation rate, Case II
45 behaviour is observed, and²⁸ n = 1. This case typically occurs when the permeant has a high
46 activity, so that swelling of the polymer film may occur in the region exposed to the donor cell,
47 with the permeant penetration front at equilibrium concentration advancing at a constant
48 velocity through the un-penetrated, glassy polymer core that is preceded by Fickian diffusion.
49 A characteristic of this behaviour is the effect of polymer history, in addition to the
50
51
52
53
54
55
56
57
58
59
60

1
2
3 manifestation of concentration-dependent diffusion coefficients. Under certain
4 conditions,^{24,26} Case II behaviour can evolve into the Super Case II category, for which $n > 1$.
5
6

7
8 It follows that, for the case when the experimental temperature (T) is lower than the glass
9 transition temperature (T_g), steady-state measurements may not afford accurate estimates of
10 the diffusion coefficient or even permeability coefficient,²⁹ as these may depend on polymer
11 history. Nevertheless, it follows that the temporal dependence of the permeant flux across the
12 membrane (the “waveshape”), which is rarely routinely reported in graphical form within the
13 literature, may afford valuable insights into the molecular mechanisms underpinning the
14 permeation process *per se*. In contrast, when the experimental temperature is larger than the
15 glass transition temperature, diffusion through the polymer should become rate-determining,
16 and therefore flux transients should follow the well-known Fickian diffusion models (*q.v.*
17 Figure 1a). We have found several flux transient waveshapes in the literature, made at
18 temperatures above the glass transition point and which depict unusual features, including
19 the occurrence of a non-stationary state at long times.²⁷ An example, taken from the work by
20 Flaconnèche *et al.*³⁰ for the permeation of methane/carbon dioxide mixtures through medium
21 density polyethylene (T_g in the range -125 to -35 °C)³¹ at an experimental temperature of 80 °C
22 at *ca.* 100 bar is depicted in Figure 1b. These data were collected using a constant pressure
23 permeation method, and it is clear that steady-state is never actually established over the
24 course of the measurement: the permeation traces tend to decrease with time. Note that
25 changing the permeant from CO_2 to methane provides similar characteristics, and in both
26 cases, there is a hint of a steady state in the flux transient around 5 h into the first flood of the
27 polymer membrane. The corresponding cumulative volume plots (Figure 15 of reference 30)
28 do not show any detectable change in slope for times greater than 5 h, and the authors did not
29 comment on the flux transients in their data. Nevertheless, this suggests there may be an
30 interaction between the polymer and the permeating species. Similar data are reported for
31 aromatic permeation through high density polyethylene membranes,³² which was modelled
32 with the assumption of a time-dependent diffusion coefficient; in other experiments, using
33 acrylate polymers (for which T_g is comparable with ambient temperature), the dual-sorption
34 model was observed to fit non-steady state flux transients for the permeation of laurel
35 pyroglutamate,²⁷ as might be anticipated from Frisch’s taxonomy.²⁴ However, for the case of
36 polydimethylsiloxane cross-linked at 75 °C, for which the melting point³³ is -40 °C, carbon
37 dioxide permeation at 30 °C gives rise to “split-wave” flux transients (Figure 1c).³⁴ There is
38 some ambiguity with the origin of the shape of the permeation curves, since the concentration
39 was determined by a mid-infrared spectral sensor, the accuracy and stability of which were
40 not disclosed; the decrease in the rate of change of concentration after about 80 min is
41 potentially due to the approach to equilibrium between the mixing chamber and the chamber
42 housing the gas sensor (*q.v.* Figure 3 of reference 34). Nevertheless, the authors did not
43 comment on the form of the permeation curves. Experimental work in our own laboratories,
44 involving CO_2 permeation (at 80 °C and 200 bar gauge) through 1.0 mm thick
45 polyvinylidene fluoride (PVDF) or polyamide-nylon 6 (PA66) membranes (see reference 35
46
47
48
49
50
51
52
53
54
55
56
57
58
59
60

1
2
3 and Supporting Information S1 for experimental details) give rise to two types of permeation
4 flux transient (Figure 1d) that differ by an order of magnitude at long time (*ca.* 200 h) and
5 hold different shapes – CO₂ flux through PVDF increases with time (Figure 1d(i)); CO₂ flux
6 through PA66 decreases with time (Figure 1d(ii)) – we will comment on this later within this
7 paper. Clearly, in all four cases, non-Fickian permeation waveshapes are observable when
8 membrane relaxation rates are expected to be faster than (or at least comparable to)
9 membrane transport rates, and it is not possible to predict, *a priori*, which polymer will give
10 rise to non-classical flux transients with a given permeant. Nor is it readily ascertainable, post
11 experiment, to discover and understand the physicochemical whys and wherefores of the
12 occurrence of such experimental anomalies, let alone deduce accurate estimates of the
13 permeant diffusion coefficient within the polymer membrane.
14
15
16
17
18
19

20 In this paper, we investigate this type of behaviour, where clearly “ideal” Fickian diffusion
21 cannot explain the experimental permeation flux transient waveshape. We postulate that,
22 above the glass transition temperature, whilst the polymer relaxation rate is much faster than
23 that for permeant diffusion, *molecular interactions between the permeant and membrane*
24 *are significant, so that the system is better described as a regular, and not ideal, solution,*
25 *except at infinite dilution.* Accordingly, we adapt regular solution theory to model the activity
26 coefficient of the permeant, and additionally consider the effects of both transport of the
27 permeant in the acceptor compartment, and the interfacial partition kinetics of the permeant
28 across the membrane | acceptor cell boundary. We demonstrate that the variety of anomalous
29 permeation flux transient waveshapes observed experimentally (*q.v.* Figure 1) are able to be
30 reproduced under particular conditions being imposed, and *only exist* when either attractive
31 or repulsive interactions occur between the permeant and the polymer membrane.
32 Furthermore, we adapt the simulated results to furnish algorithmic protocols suitable for use
33 by experimental measurement scientists and engineers, so as to report *self-consistent* values
34 of the permeant diffusion coefficient *at infinite dilution* (*viz.* the Fickian diffusion coefficient).
35
36
37
38
39
40
41
42
43
44
45
46
47
48
49
50
51
52
53
54
55
56
57
58
59
60

Theory

In this section, we review the classical case for one-dimensional permeation within polymer membranes, where the diffusion coefficient of the permeant is constant, and then introduce the case where the permeant within the membrane forms a regular solution, so that its diffusion coefficient varies with its concentration.

Classical Permeation Model

We first re-examine the Fickian theoretical model for slow, uniform, one-dimensional diffusion of a permeant through a membrane separating an donor compartment and an acceptor phase, as illustrated in Figure 2a. We assume that the system comprises a constant pressure permeation cell, with no membrane swelling during the experiment, and that the donor is an infinite source of permeant molecules, and so is not depleted on the timescale of the experiment. At the other face of the membrane, the permeant is rapidly taken up by the acceptor phase, so that the permeant concentration is maintained at zero. Accordingly, the transport equation to solve for this problem is given in equation (1):

$$\frac{\partial c}{\partial t} = D \frac{\partial^2 c}{\partial x^2} \quad (1)$$

where c is the permeant concentration, t is the temporal variable, x is the spatial variable and D is the diffusion coefficient of the permeant at infinite dilution. This is Fick's second law, and is subject to the boundary conditions,

$$\begin{aligned} t \leq 0, x = 0 & \quad c = c_0 \\ t \leq 0, x > 0 & \quad c = 0 \\ t > 0, x = 0 & \quad c = c_0 \\ t > 0, x = b & \quad c = 0 \end{aligned}$$

in which the infinite donor source of the permeant is located at $x = 0$, and the membrane thickness is b . It follows that, after a short incubation time, a steady-state concentration profile of the permeant is established, in accordance with¹⁵ equation (2),

$$c = c_0 - c_0 \frac{x}{b} + \frac{2}{\pi} \sum_{n=1}^{\infty} \frac{c_0}{n} \sin\left(\frac{n\pi x}{b}\right) \exp\left(-\frac{Dn^2\pi^2 t}{b^2}\right) \quad (2)$$

It is clear that as $t \rightarrow \infty$, the permeant follows a linear concentration distribution, as illustrated in Figure 2b, which was simulated numerically – the summation converges rapidly, and $n = 1000$ is a sufficient approximation for $n \rightarrow \infty$. At any time, the permeant flux, i , into the acceptor compartment is given by Fick's first law:

$$i = -D \left(\frac{\partial c}{\partial x} \right)_{x=b} = \frac{Dc_0}{b} + \frac{2Dc_0}{b} \sum_{n=1}^{\infty} (-1)^n \exp\left(-\frac{Dn^2\pi^2 t}{b^2}\right) \quad (3)$$

This yields the classical flux transient depicted in Figure 2c, where it is seen that a sigmoidal curve develops after a short time interval (during which the ratio $\frac{M_t}{M_\infty} \propto \sqrt{t}$) into a steady-state flux, given by $\frac{Dc_0}{b}$, and indicating that, all other things being equal, faster diffusion

through the membrane (larger D) and/or thinner membranes (smaller b) give rise to the largest flux at steady-state for a given permeant concentration in the donor compartment.

The flux affords the rate at which permeant molecules pass through unit area of the membrane (units of $\text{mol m}^{-2} \text{s}^{-1}$). However, a popular alternative examines the mole flow - the amount of permeant that emerges into the acceptor compartment from unit membrane area at any given time, $Q(t)$, in units of mol m^{-2} . It follows from equation (3) that integration with respect to time affords the following expression, using the boundary condition $Q(0) = 0$.

$$\frac{Q(t)}{c_0 b} = \frac{Dt}{b^2} - \frac{1}{6} - \frac{2}{\pi^2} \sum_{n=1}^{\infty} (-1)^n \exp\left(-\frac{Dn^2 \pi^2 t}{b^2}\right) \quad (4)$$

The fraction $\frac{1}{6}$ in equation (4) arises from the expression $\frac{2}{\pi^2} \sum_{n=1}^{\infty} \frac{(-1)^n}{n^2}$, since $\sum_{n=1}^{\infty} \frac{(-1)^n}{n^2} = \frac{\pi^2}{12}$.

Figure 2d illustrates plots of $Q(t)$ against t . It is clear that as $t \rightarrow \infty$, equation (4) approaches the line $Q(t \rightarrow \infty) = \frac{Dc_0}{b} \left(t - \frac{b^2}{6D}\right)$, which has an intercept, L , on the temporal axis of $L = \frac{b^2}{6D}$.

This value is known as the “time lag”; its construction, which exploits *both* steady- and non-stationary state, is a convenient method to determine the permeant diffusion coefficient, provided the membrane thickness is known. Moreover, if the sorption coefficient, K^L , for equilibrium between the donor source and the membrane is known, the permeability coefficient, P_e is readily deduced,¹ since $P_e = K^L D$. Furthermore, the permeant solubility, S , in the membrane phase is readily estimated through³⁶ $P_e = SD$.

Unfortunately, as identified by Frisch,²³ this simple construction, though attractive, requires lengthy calculations for the case when the permeant diffusion coefficient is not constant, but rather a function of the permeant concentration in both space and time. Indeed, for this case, *there is no simple route for the experimentalist* to determine whether the observed permeation flux transient is of a correct form, nor is there any self-consistent route to estimate the diffusion coefficient at infinite dilution. Moreover, under the conditions of no interactions occurring between the membrane and the permeant, the variable diffusion coefficient of the permeant can only be interpreted in terms of *mechanical structural changes* of the membrane, or its chemical reaction with the permeant. Accordingly, we next demonstrate that *variable diffusion coefficients of the permeant through the membrane may arise from the presence of membrane-permeant interactions, and these may have a significant influence on the permeant transient waveshape*.

Regular Solution Theory

The experimental results of apparently non-Fickian diffusion within a variety of polymer films at temperatures much greater than their glass transition temperatures given in Figure 1, coupled with the fitting of some of the data with the dual sorption mechanism, encourages us

to propose a model in which the permeant species has some affinity for the polymer membrane. However, this interaction must be sufficiently weak to allow for *all* of the permeant molecules to diffuse through the membrane, rather than some becoming irreversibly adsorbed and immobile within the polymer film. Thermodynamically, this encourages us to consider the case where the permeant-polymer mixing enthalpy is non-ideal (non-zero), whilst the entropy change on mixing is maintained at its ideal value, *viz.*, the permeant-polymer system is described as a regular solution.³⁷ Accordingly, the activity, *a*, of the permeant in the polymer film will only approach the permeant concentration, *c*, in the limiting case of an infinitely dilute solution. It follows that the one-dimensional permeant flux, *j*, through the membrane,

$$j = -\frac{Dc}{RT} \frac{\partial \mu}{\partial x} \quad (5)$$

in which *D* is the permeant diffusion coefficient at infinite dilution (corresponding to the constant Fickian diffusion coefficient), *R* is the molar gas constant, *T*, the absolute temperature, μ is the chemical potential of the permeant and *x* is, as before, the one-dimensional spatial variable, can be recast in terms of a concentration-dependent effective diffusion coefficient, *D_{eff}*:

$$j = -D_{eff} \frac{\partial c}{\partial x} \quad (6)$$

where

$$D_{eff} = D \left(1 + \frac{\partial \ln \gamma}{\partial \ln c} \right) \quad (7)$$

with the activity coefficient, γ , being the constant of proportionality between the permeant activity and its concentration, *viz.*, $a = \gamma c$. For regular solutions, the activity coefficient is described³⁷ through an exponential quadratic dependence on the mole fraction of permeant in the polymer (*x_q*):

$$\ln \gamma = Z \left(1 - x_q \right)^2 \quad (8)$$

where $Z = \frac{zw}{RT}$ is a single interaction parameter that accounts for both attractive ($Z < 0$) and repulsive ($Z > 0$) interactions between the permeant and the polymer; in the regular solution, the permeant and polymer system is considered to exist as a lattice, so that a single permeant molecule interacts with each of its *z* neighbours, with average molar energy, *w*. This interaction parameter is then an effective statistical ratio of the permeant-polymer interactions to thermal energy; its use is highly convenient for our purposes, since it typically varies over the range $-2 < Z < 2$, with $Z = 0$ corresponding to the ideal (Fickian) case, and $Z > 2$ affording a permeant-polymer system that is incompletely miscible.³⁷

In view of the central rôle of the interaction parameter, *Z*, in this work, it is important that it is clearly defined and related to other polymer-solvent or polymer-permeant interaction

parameters, such as the Flory-Huggins interaction parameter, χ .³⁸ In the next section we develop a relationship between Z and χ .

Relationship between Regular Solution Theory and Flory-Huggins Theory

Regular solution theory gives an expression, with its attendant approximations, for the activity coefficient γ_1 of component 1 dissolved in component 2 of the form,^{38a}

$$RT \ln \gamma_1 = V_{m1} (1 - v_1)^2 (\delta_1 - \delta_2)^2 \quad (9)$$

where V_{m1} is the partial molar volume of species 1; v_1 its volume fraction; and δ_1 and δ_2 the solubility parameters of components 1 and 2, defined by,

$$\delta_i = \sqrt{\frac{\Delta U_i}{V_{mi}}} \quad (10)$$

in which ΔU_i is the energy of evaporation of species i at constant temperature.^{38b} The Flory-Huggins interaction parameter, χ , has been related to δ_1 and δ_2 by Zielinski and Duda:^{38e}

$$\chi = 0.35 + \frac{V_{m1}}{RT} (\delta_1 - \delta_2)^2 \quad (11)$$

which yields a relationship between γ_1 and χ ,

$$\ln \gamma_1 = (\chi - 0.35) (1 - v_1)^2 \quad (12)$$

Since the volume fraction v_1 and the mole fraction x_1 are related by

$$v_1 = \frac{\alpha x_1}{\alpha x_1 + 1 - x_1} \quad (13)$$

where $\alpha = \frac{V_{m1}}{V_{m2}}$, it follows that

$$\ln \gamma_1 = \frac{(\chi - 0.35)}{(\alpha x_1 + 1 - x_1)^2} (1 - x_1)^2 \quad (14)$$

Comparison of equation (14) with equation (8) indicates that χ and Z are related by,

$$Z = \frac{(\chi - 0.35)}{(\alpha x_1 + 1 - x_1)^2} \quad (15)$$

Thus, for the permeation of gases through polymers in the absence of swelling, it is expected that $x_1 \ll 1$ and therefore $Z \approx \chi - 0.35$. Thus, in view of the large number of values of the Flory-Huggins interaction parameter χ published for polymer-solute systems,³⁹ equation (15) and its approximate form represent an important route for the prediction of the regular solution interaction parameter Z used in this work.

Regular Solution Permeation Model

In the current study, we assume a constant pressure permeation cell depicted in Figure 3 (where the co-ordinate system is defined) – *no swelling of the membrane film is considered to occur during the permeation process*, and we consider the interaction parameter as being

constant (distance invariant) for the permeant-polymer system, but in the range $-1.5 \leq Z \leq 1.5$, so that the permeant-polymer system forms a single phase. As there is no change in volume, the mole fraction of the permeant is simply the ratio of the permeant concentration to that corresponding to the initial concentration, c_0 , of the permeant at the edge of the polymer film (at the boundary with the infinite source) added to the concentration of the polymer (or polymer segments) in the membrane, c_{poly} : $x_q = \frac{c}{c_0 + c_{poly}} = q$. Thus, substitution of equation

(8) into equation (7) reveals the concentration-dependence of the permeant diffusion coefficient in the polymer:

$$D_{eff} = D \{1 - 2Zq(1 - q)\} \quad (16)$$

Clearly, when $Z = 0$, the Fickian case is re-established: $D_{eff} = D$. It follows that Fick's second law for the rate of change of permeant concentration within the polymer film is given as:

$$\frac{\partial c}{\partial t} = -\frac{\partial j}{\partial x} = D_{eff} \frac{\partial^2 c}{\partial x^2} + \frac{\partial c}{\partial x} \frac{\partial}{\partial x} (D_{eff}) \quad (17)$$

or, equivalently,

$$\frac{\partial q}{\partial t} = D \{1 - 2Zq(1 - q)\} \frac{\partial^2 q}{\partial x^2} - 2ZD(1 - 2q) \left(\frac{\partial q}{\partial x} \right)^2 \quad (18)$$

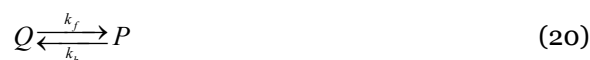
It is this equation that is to be solved for transport through the membrane. However, as illustrated in Figure 3, there are other compartments in which permeant species can be transported, and to understand the boundary conditions imposed, we next describe the geometry of the permeation cell.

For simplicity, we consider the permeation cell as comprising three adjacent layers, donor compartment | membrane | acceptor compartment, $q.v.$ Figure 3, with interfaces that are infinitesimally thin.⁴⁰ We assume that the polymer membrane is uniform and free from defects or micro-cracks.⁴¹ We assume that the permeant *in the donor compartment* rapidly equilibrates with the membrane, defined by the Henry's law-type equilibrium constant H :

$$H = \frac{c_{membrane}}{c_{donor}} \quad (19)$$

where $c_{membrane}$ is the permeant concentration in the membrane at the donor | membrane interface, and c_{donor} is the bulk concentration of the permeating species in the donor compartment. Moreover, we assume that the donor compartment is an infinite, well-mixed source, so that transport within the donor compartment resulting from permeant sorption by the membrane is negligible. It follows that $c_{membrane} = c_0$ at all times at this interface. Accordingly, we neglect the donor compartment from further consideration and define $x = 0$ as the donor compartment | membrane interface, as indicated in Figure 3. The membrane thickness is, as before, denoted by the symbol b , such that when $x = b$, the membrane contacts the acceptor compartment ($q.v.$ Figure 3). In this work, we assume that the acceptor compartment contains a static, semi-infinite, incompressible fluid (gas or liquid of constant

density), so that the only transport of the permeant in this fluid is through diffusion. Furthermore, we assume that this process merely occurs through Fickian diffusion with constant diffusion coefficient, D_p , and that natural convective processes do not occur.⁴² In order to account for the equality of the flux of the permeating species between the membrane and the acceptor compartment, and in recognising that the bathing environment of the permeant is likely different in both zones, we treat the permeant as two separate species: that in the membrane is species Q, whilst the species emerging into the acceptor compartment is species P. Thus, the following chemical process is established at the membrane | acceptor compartment interface.



where k_f and k_b are heterogeneous rate constants for species transfer across the membrane | acceptor interface. If the desorption-sorption kinetics are rapid at this interface compared with the measurement time, equilibrium is established at all times, so that we may describe the concentrations of the permeant *in the membrane and acceptor compartment phases* through the partition coefficient, K_P :

$$K_P = \frac{c_{\text{acceptor}}}{c_{\text{membrane}}} = \frac{c_P}{c_Q} = \frac{k_f}{k_b} \quad (21)$$

in which c_J refers to the concentration of species J at the interface ($x = b$). We are interested in examining the case where the interfacial kinetics across this membrane | acceptor boundary are varied, so that equilibrium may not always be established at the membrane | acceptor compartment interface.

For our model, these assumptions translate into the following transport equations solved subject to spatio-temporal boundary conditions.

In the membrane:

$$\frac{\partial q}{\partial t} = D \left\{ 1 - 2Zq(1-q) \right\} \frac{\partial^2 q}{\partial x^2} - 2ZD(1-2q) \left(\frac{\partial q}{\partial x} \right)^2 \quad (18)$$

In the acceptor compartment:

$$\frac{\partial p}{\partial t} = D_p \frac{\partial^2 p}{\partial x^2} \quad (22)$$

Boundary conditions:

$$\begin{aligned}
 & t \leq 0 \\
 & \quad x = 0 \quad c_Q = c_0; \quad c_P = 0 \\
 & \quad x > 0 \quad c_Q = 0; \quad c_P = 0 \\
 & t > 0 \\
 & \quad x = 0 \quad c_Q = c_0; \quad c_P = 0 \\
 & \quad 0 < x < b \quad j_Q = -D_{\text{eff}} \frac{\partial c_Q}{\partial x}; \quad j_P = 0 \\
 & \quad x = b \quad D_{\text{eff}} \frac{\partial c_Q}{\partial x} = D_P \frac{\partial c_P}{\partial x} = k_b c_P - k_f c_Q \\
 & \quad b < x < \infty \quad j_Q = 0; \quad j_P = -D_P \frac{\partial c_P}{\partial x} \\
 & \quad x \rightarrow \infty \quad j_Q = 0; \quad j_P = 0
 \end{aligned}$$

The no-flux boundary condition given as $x \rightarrow \infty$ is, in reality, specified as the distal edge of the acceptor compartment (the proximal edge being the membrane | acceptor interface); for the simulations considered herein (*vide infra*), this is considered as being four times the size of the membrane (*q.v.* Figure 3).

We are interested in measuring the permeation flux (i) across the membrane | acceptor compartment, which is given by equation (16):

$$i = -D_{\text{eff}} \left(\frac{\partial c_Q}{\partial x} \right)_{x=b} = -D_P \left(\frac{\partial c_P}{\partial x} \right)_{x=b} \quad (23)$$

and is readily deduced from numerical solution of equations (18) and (23). This was achieved through finite difference simulation within a uniformly spaced time and space grid (parameterised by dummy variables k and j, respectively), with linearization of the quadratic terms,⁴³ *viz.*,

$$a_j^k b_j^k \approx a_j^k b_j^{k-1} + a_j^{k-1} b_j^k - a_j^{k-1} b_j^{k-1} \quad (24)$$

using implicit kinetics. The effective diffusion coefficient in the membrane phase was computed using explicit values of the concentration of species Q. Since equations (18) and (22) are coupled at the membrane | acceptor compartment interface, the partial differential equations were solved using a pentadiagonal matrix algorithm outlined in earlier work.^{42b} The permeation flux was then computed from equation (23) through forward differences, and recorded as a function of time.

In order to generate general waveshape transients for the permeation problem from the specific solutions simulated, we introduce the following dimensionless variables.

Time:

$$\tau = \frac{\pi^2 D t}{b^2} \quad (25)$$

Space:

$$y = \frac{x}{\sqrt{\pi Dt}} = \frac{x}{b\sqrt{\tau/\pi}} \quad (26)$$

Concentrations:

$$q = \frac{c_0}{c_0 + c_{poly}} = \frac{c}{c_0 + c_{poly}}; \quad p = \frac{c_p}{c_0 + c_{poly}} \quad (27)$$

Diffusion coefficients:

$$\delta = \frac{D_{eff}}{D}; \quad \varepsilon = \frac{D_p}{D} \quad (28)$$

Acceptor phase permeation interfacial kinetics:

$$\Lambda_f = k_f \frac{\sqrt{\vartheta}}{\sqrt{D}} = \frac{k_f b}{\pi D} \sqrt{\tau_\vartheta}; \quad \Lambda_b = \frac{k_b b}{\pi D} \sqrt{\tau_\vartheta} \quad (29)$$

Permeation flux:

$$\psi = \frac{ib}{Dc_0} \quad (30)$$

In equation (29), ϑ represents the total time over which the permeation transient is recorded (the experimental measurement time), with τ_ϑ being the corresponding dimensionless time, determined from equation (25) with $t = \vartheta$. Note that the normalising parameter for permeation flux in equation (30) is the steady-state flux under ideal Fickian conditions, which corresponds to $\psi = 1$.

Computing

Numerical simulation was undertaken *via* program encoding in GNU FORTRAN using the freely available G77 compiler, with double-precision variables,⁴⁴ and was executed on an Intel Pentium processor (of speed, 2.4 GHz, with 1.98 GB of random access memory) and employed finite difference grid comprising 10000 temporal nodes and 50000 spatial nodes; the latter were divided with the membrane comprising the first fifth of the spatial nodes and the acceptor phase the rest. For typical simulations, the measurement time, ϑ , was 100 s, with Fickian diffusion coefficients of $D = 10^{-9} \text{ m}^2 \text{ s}^{-1}$ (inside the membrane) and, in the acceptor phase, $-11 \leq \lg(D_p/\text{m}^2 \text{ s}^{-1}) \leq -4$, for a one-dimensional box size of 1.0 mm, *viz.* just over three times the diffusion length of permeant in the membrane under the experimental timescale. Accordingly, the membrane thickness, b , was fixed at 0.2 mm (corresponding to one-fifth of the length of the total box simulated), and for ease, the permeant concentration at the donor compartment | membrane edge was fixed at $c_0 = 1.0 \text{ mM}$. The membrane interaction parameter, Z , was varied over the range $-1.5 \leq Z \leq 1.5$, with the rate constants for permeant transfer across the membrane | acceptor phase interface in the range $-6 \leq \lg(k_f/\text{m s}^{-1}) \leq 0$ and $-6 \leq \lg(k_b/\text{m s}^{-1}) \leq 0$ corresponding to $-0.5 \leq \lg(\Lambda_i) \leq 5.5$ ($i = f$ or b), thereby spanning the

1
2
3 kinetically reversible (fast transfer), kinetically irreversible (slow transfer) and kinetically
4 quasi-reversible regimes (*vide infra*). Simulations of a single dimensionless flux transient
5 took *ca.* 75 s of CPU time. Data were imported and manipulated using Matlab R2013a
6 (Mathworks) for graphical processing of the data.
7
8
9
10
11
12
13
14
15
16
17
18
19
20
21
22
23
24
25
26
27
28
29
30
31
32
33
34
35
36
37
38
39
40
41
42
43
44
45
46
47
48
49
50
51
52
53
54
55
56
57
58
59
60

Results and Discussion

We first present the effect of regular solution based molecular interactions on permeant flux transient wavelshapes and their validated comparison with the classical case, and subsequently identify and quantify the nuances in permeation transient wavelshape due to either slower transport in the acceptor compartment, or slow rates of interfacial transfer across the membrane | acceptor boundary.

Effect of Molecular Interactions on Permeation Flux Transients

Figure 4a illustrates permeation flux transients corresponding to the permeation of a small gaseous molecule through a membrane from an infinite source and moving into a stationary gas compartment (the acceptor cell). This corresponds to the idealised case where transport in the acceptor compartment is fast, so that the concentration of permeant at the acceptor side of the membrane is essentially zero; Figure 4a was simulated with $D = 10^{-9} \text{ m}^2 \text{ s}^{-1}$ and $D_p = 1.5 \times 10^{-4} \text{ m}^2 \text{ s}^{-1}$. The latter corresponds to the typical diffusion coefficient of gaseous molecules at room temperature and pressure. Furthermore, we assume that the partition kinetics of the permeant from the membrane and into the receiving cell are fast ($k_f = k_b = 1.0 \text{ m s}^{-1}$). This enables the comparison of the permeation flux transients simulated for the ideal case ($Z = 0$) to be compared with analytical theory (equation (3)), and checked for accuracy in convergence. Indeed, as illustrated in Figure 4a, there is an excellent match between $Z = 0$ and the dimensionless form of equation (3), validating the convergence of the simulation.

The variation of the interaction parameter to non-ideal values reveals three features. First, *steady state signals are observed at all values of the interaction parameter at long time periods*. Second, attractive polymer-permeant interactions ($Z < 0$) produce a flux that is greater than the ideal case, whilst repulsive interactions ($Z > 0$) reduces the flux at steady state. Moreover, steady-state is reached *sooner* for attractive interactions and *later* for repulsive ones, compared with the ideal scenario of no interactions. At first sight, this appears to be incongruent with what may be expected: attractive interactions would be expected to *reduce* the tendency of the permeant to leave the membrane film. However, the permeation flux, by definition, is a product of both the effective diffusion coefficient of the permeant within the membrane, and the concentration gradient at the membrane | acceptor compartment boundary, as given by equation (23). Since non-ideal effective diffusion coefficients are non-constant (equation (16)) and depend on the permeant concentration, it is thus insightful to consider the spatio-temporal variation of both diffusion coefficient and permeant concentration within the membrane. Figures 4b-d illustrate the spatial profile for these at steady-state (corresponding to a simulation time of $\vartheta = 100 \text{ s}$). In both ideal and non-ideal cases, the permeant concentration decreases across the membrane, reaching zero at the interface with the receiving cell, thereby affording the stationary state, and constancy of the permeation flux (Figure 4b). As expected (*vide supra*), in the ideal case there is constancy

1
2
3 in the reduction of the permeant concentration in the membrane from donor to acceptor
4 edges. However, the non-ideal cases deviate from this, with a greater discrepancy resulting
5 from repulsive ($Z > 0$) interactions. Nevertheless, these profiles reveal a point of inflexion in
6 the steady-state concentration profile occurring at the membrane mid-point, whence the
7 permeant concentration is identical (and equal to one half of c_0) irrespective of the nature of
8 the molecular interactions, so that the membrane is best considered as comprising two halves.
9 In the donor-facing half, attractive interactions encourage more rapid uptake of the permeant
10 into the membrane from the donor compared with the ideal characteristic, whilst repulsive
11 interactions retard this ingress; conversely, in the acceptor-facing half, attractive interactions
12 lower the rate of permeant transport across the edge of the membrane, resulting in higher
13 concentrations of permeant than the ideal case, whilst repulsive interactions speeds up the
14 removal of permeant into the acceptor phase. Accordingly, the permeant concentration is
15 greater than ideal for attractive interactions, but smaller than ideal for the repulsive ones,
16 resulting in a permeation flux from membrane to acceptor cell that is much greater for
17 attractive interactions compared with the ideal case, and a smaller flux when the interactions
18 are repulsive. This explains the magnitude of the steady-state signals observed, and is also
19 reflected in the ordering of the analyte concentration in the acceptor phase being attractive
20 interactions > ideal (no interactions) > repulsive interactions, *q.v.* Figure 4c.
21
22
23
24
25
26
27
28
29

30 The effect of this on the diffusion coefficient of the permeant within the membrane is
31 dramatic, as illustrated in Figure 4d. For the case when there are no interactions between
32 membrane and permeant, the diffusion coefficient of the permeant is constant. The
33 occurrence of molecular interactions causes the diffusion coefficient to peak in a maximum
34 (attractive interactions) or reduce to a minimum (repulsive interactions) at the membrane
35 mid-point, compounding the analysis above. The more dramatic variation in the diffusion
36 coefficient across the membrane for the case of repulsive interactions is rationalised by their
37 greater destabilising effect of the system, corresponding to greater than unity activity
38 coefficients (*q.v.* equation (8)) compared with the stability enhancing (*viz.* sub-unity activity
39 coefficients) attractive interactions. Indeed, the quadratic dependence indicated in equation
40 (8) underpins the parabolic nature of the diffusion coefficient variation observed, and directly
41 leads to the compartmentalisation of the membrane into donor-facing and acceptor-facing
42 halves; indeed, the variations of D_{eff}/D with x at various Z illustrated in Figure 4d can largely
43 be determined from equation (16) with $q = 1 - x/b$, so that the maximum or minimum value of
44 D_{eff}/D is $1 - 1/2Z$ and occurs at $q = 1/2$.
45
46
47
48
49
50
51
52

53 It follows that the time taken to reach steady-state concentration profiles varies with the type
54 and extent of the interactions: attractive interactions enable a faster approach to zero
55 permeant concentration at the membrane | acceptor edge (for rapid acceptor phase transport)
56 than the ideal and the repulsive interactions. This is as expected, for the reasons outlined
57 above: attractive interactions lead to sub-unity activity coefficients and therefore faster
58 diffusion regimes through the membrane compared with repulsive interactions. This enables
59
60

us to develop the algorithmic decision tree exhibited in Figure 4e as a toolkit for the experimental measurement scientist to estimate the diffusion coefficient of the permeant at infinite dilute (D), using the data extracted from the dimensionless permeation transients provided in Table 1. This method relies on the occurrence of steady-state permeation transients in the experiment, and exploits the ratio of the diffusion coefficients extracted from the limiting flux (D_{lim}) to that obtained from the flux at 50% of the of the steady-state value (D_{50}) as a “self-consistency index” (SCI), *viz.*

$$SCI = \frac{D_{50}}{D_{\text{lim}}} \quad (31)$$

First, it is assumed that ideal diffusion occurs and the dimensionless permeation flux at steady-state is unity. Equation (30) then allows the immediate estimation of D_{lim} . From the experimental time taken since the start of the permeation transient to reach steady-state, using the value of the corresponding dimensionless time, τ_{50} , given in Table 1 for the ideal case ($Z = 0$), D_{50} may be estimated using equation (25). The ratio of these two diffusion coefficients is the self-consistency index, equation (31), which equals unity within a threshold tolerance (typically 0.05%), if $Z = 0$, suggesting no interactions occur between the permeant and the membrane. Repulsive interactions tend to lead to SCI values greater than unity, whilst attractive interactions afford values smaller than unity. This then allows the experimentalist to determine in which direction Z should be shifted, *viz.* greater than zero or less than zero, so that new iterative estimates of both the dimensionless limiting permeation flux (ψ_{lim}) and the adimensional time taken to reach 50% of the steady flux (τ_{50}) may be computed from the data in Table 1, *viz.*

$$\begin{aligned} \psi_{\text{lim}} &= 1 - \frac{1}{3}Z \\ \tau_{50} &= 1.4052e^{0.2602Z}; \quad R^2 = 0.99387 \end{aligned} \quad (32)$$

with the iteration completing until the SCI value approaches unity (within the required tolerance), so that the arithmetic mean of the two diffusion coefficients may be reported, together with the interaction parameter.

Having thus examined the effect of the interaction parameter on the permeation flux transient waveshape, we next investigate the changes to the waveshape that occur when transport within the acceptor compartment approaches that within the membrane.

Effect of Slow Transport in the Acceptor Cell

Slow transport within the acceptor cell corresponds to the case where $D_p \leq D$, so that the rate-limiting step is no longer diffusion through the membrane, but, rather transport within the acceptor cell, provided the partition coefficient and kinetics at the membrane | acceptor cell interface are large and rapid, respectively. Figure 5a illustrates permeation transients that occur when $D_p = 15D$, with all other parameters remaining as for those depicted in Figure 4a. Several trends are observable when compared with the waveshapes shown in Figure 4a. First,

the slower movement of species in the receiving compartment causes a reduction in the size of the permeation flux transient than would otherwise be observed – less material is apparently transferred across the membrane | acceptor interface. This makes sense since the boundary condition at this interface is of the Neumann kind, and is the case of flux equality; the permeation flux depends on the speed at which material is removed from the acceptor side of the boundary. Second, all other things being equal, it is only the case of no interactions between the permeant and the membrane that enables the occurrence of a stationary state in permeant concentration profile within the same timescale as that for faster diffusion (Figure 4a); attractive membrane interactions lead to the observation of a *peak maximum* in the flux transient, whilst repulsive membrane interactions furnish a slowly rising wavelike shape, which may manifest as *split waves* (q.v. Figure 5b, *vide infra*).

Since both of these effects stem only from the large deviations of non-zero concentration at the acceptor cell edge of the membrane, it follows that the easiest way for an experimentalist to deal with peak wavelike shapes is to repeat the experiment, albeit ensuring a faster transport rate in the acceptor compartment. If the acceptor phase is a fluid under quiescent conditions (as modelled in this work), this means using a less viscous fluid;⁹ conversely, if the receiving medium is a flowing fluid stream, as in the most frequently used experimental arrangement, this requires using a higher volumetric flow rate of the fluid stream, so that the permeant concentration at the acceptor side of the membrane is maintained as close to zero as required for analysis through the algorithm given in Figure 4e.

In some experimental cases, it is not readily achievable to change the mass transport in the acceptor cell, but it may be more facile to remove the infinite source. Under these conditions, the flux transient recorded is the equivalent of that observed during a “double-step” technique exploited extensively in electrochemistry, and provides valuable information pertaining to diffusion through the membrane, since, during the second step, the boundary condition at the donor cell | membrane interface is at the transport limit. Accordingly, for this second step (taken arbitrarily to be of duration ϑ), equations (18) and (22) are solved, as before, but with the following additional boundary conditions.

Boundary conditions :

$$\vartheta < t \leq 2\vartheta$$

$$x = 0 \quad c_Q = c_P = 0$$

$$0 < x < b \quad j_Q = -D_{eff} \frac{\partial c_Q}{\partial x}; \quad j_P = 0$$

$$x = b \quad D_{eff} \frac{\partial c_Q}{\partial x} = D_P \frac{\partial c_P}{\partial x} = k_b c_P - k_f c_Q$$

$$b < x < \infty \quad j_Q = 0; \quad j_P = -D_P \frac{\partial c_P}{\partial x}$$

$$x \rightarrow \infty \quad j_Q = j_P = 0$$

Figure 5b and Supporting Information S2 provides three-dimensional plots illustrating the waveshapes of these double-step permeations as both the interaction parameter (Z) and the ratio of acceptor cell to ideal membrane transport are varied in the ranges $-1.5 \leq Z \leq 1.5$ and $-3 \leq \lg \left\{ \frac{D_p}{D} \right\} \leq 5$. These results demonstrate several nuances in addition to those already described: first, *peaks in the first permeation flood are only observed for the case of attractive ($Z < 0$) and ideal ($Z = 0$) interactions, whenever the acceptor transport diffusion coefficient is less than approximately ten times the membrane diffusion coefficient at infinite dilution, viz. $\lg \left\{ \frac{D_p}{D} \right\} \leq 1$; second, the reverse permeation process may also exhibit peaks, although these occur mainly when the diffusion coefficients are most similar, viz. $\lg \left\{ \frac{D_p}{D} \right\} \approx 0$; last, *highly repulsive interactions ($Z > 0$) give rise to split permeation waveshapes with two turning points during the first penetration of the membrane, only when diffusion in the acceptor cell becomes significantly slower than the ideal membrane diffusion, viz. $\lg \left\{ \frac{D_p}{D} \right\} \leq -1$, so that the transient is affected by the non-constant, grossly non-ideal and greater than unity activity coefficient, in addition to the slow loss of permeant at the membrane | receiving cell interface.**

It follows that, for the experimentalist to extract quantitative information from such double-step transients pertaining to membrane diffusion *and* acceptor cell diffusion, the “transport parameter,” $\frac{\psi_{\vartheta} - \psi_{2\vartheta}}{\psi_{\vartheta}}$, which only requires the measurement of the observed flux in the *acceptor cell* at the end of the first step ($t = \vartheta$) and at the end of the second step ($t = 2\vartheta$), readily enables this, as illustrated in Figure 5c. This figure may be used as a “working curve” for experimentalists. However, it is clear that, for the case of fast transport in the acceptor phase, there is no possibility to use this technique for determining the interaction parameter; rather the algorithm in Figure 4e should be used.

Hitherto, we have been interested in the case where equilibrium partitioning ($K_p = 1$) between the membrane and the receiving cell occurs with rapid heterogeneous kinetics ($\lg \Lambda_i = 5.5$; $i = f$ or b). We next examine the influence of small partition coefficients and slow heterogeneous kinetics on permeation transient waveshapes.

Effects of Variable Partition Coefficient and Membrane | Acceptor Cell Interfacial Kinetics

Figure 6a illustrates permeation flux transients under parameters identical with Figure 5a, *viz.* variable interaction parameter (Z), slow diffusion in the acceptor compartment ($D_p = 15D$), but with a reduced partition coefficient across the membrane | acceptor cell

1
2
3 interface ($K_p = 10^{-2}$ vs. 1.0) resulting from a lowered heterogeneous rate constant for the
4 partition process ($k_f = 10^{-2} \text{ m s}^{-1}$ vs. 1.0 m s^{-1}). The traces in Figure 6a appear to afford the
5 diversity of the traces indicated in Figure 1, *viz.* the occurrence of peaks and split-waves.
6 However, when compared with Figure 5a, it is clear that the decrease in heterogeneous
7 kinetics and partition coefficient markedly affect the permeation waveshape through *lowering*
8 the flux and “stretching-out” the waveshape, with, as expected attractive interactions
9 manifesting through peaks in transient, whilst repulsive interactions giving rise to split-
10 waves.
11
12
13
14
15

16 In order to remove the effects of slow transport in the acceptor cell, Figure 6b and Supporting
17 Information S3 depicts the results from simulations made under conditions of fast permeant
18 transport in the acceptor cell, with the variation of both partition coefficient ($-6 \leq \lg K_p \leq 6$)
19 and forward heterogeneous rate constant across the membrane | acceptor cell boundary ($-$
20 $0.5 \leq \lg \Lambda_f \leq 5.5$). Under these conditions, *no peaks occur in the permeation waveshapes, and*
21 *split-waves only occur when repulsive interactions (permeant activity coefficients in the*
22 *membrane being greater than unity) occur and when both the partition coefficient and*
23 *forward rate constants are small.* Since classical waveshapes are observed for the large
24 majority of the cases simulated, both the limiting permeation flux (ψ_{lim}) and time taken to
25 reach 50% of the steady-state flux (τ_{50}) of the signals in Figure 6b are reported in Table 2. It is
26 readily seen that, irrespective of the magnitude and type of the permeant interactions with the
27 membrane, at constant partition constant, as the heterogeneous kinetics for the transfer of
28 permeant from the membrane to the acceptor cell decreases, the limiting flux decreases and
29 the time taken to reach the stationary state increases. This is the underpinning manifestation
30 of slow interfacial kinetics, and is the result of “slow” transfer through the interface compared
31 with transport through the membrane, on the experimental timescale. Accordingly, it is
32 convenient to depict this, irrespective of the interaction extent and level, in terms of a kinetic
33 zone diagram – a visual representation of the regions corresponding to those where a
34 complete analysis of the kinetics must be carried out, and the areas of limiting behaviour
35 where the system does not depend on any parameter, meaning that experimental variables are
36 used to normalised the parameters, and thus a single adimensional expression of the limiting
37 flux ($\psi_{\text{lim}/g}$) or half-flux time (τ_{50}) provides what is necessary for all possible experimental
38 situations. This diagram is illustrated in Figure 6c, where it is seen that it comprises five
39 regions which reflect the level of uncertainty in the observed transient compared with those
40 obtained for the most thermodynamically favoured ($\lg K_p = 6$) and kinetically fast ($\lg \Lambda_f = 5.5$)
41 partition process between the membrane and the acceptor cell. In the pure diffusion (PD)
42 region, the values in Table 2 are within $10^{-4}\%$ of this standard; the equilibrium diffusion (ED)
43 zone maps out an uncertainty less than 1.0%, whilst that in the general kinetics area is $<10\%$.
44 As suggested by the relationships between the limiting flux and the half-flux time and the
45
46
47
48
49
50
51
52
53
54
55
56
57
58
59
60

1
2
3 interaction parameter given in Table 3, for these three zones, experimental data may be first
4 treated using the expressions given in equation (32) to estimate values of Z and D , before
5 using the more refined expressions given in Table 3 coupled with the self-consistency protocol
6 indicated in Figure 4e. In contrast, experimental data which fall in the quasi-reversible
7 equilibrium region (QRE) where the uncertainty is less than 60%, or in the pure kinetics zone
8 (PK) where split-waves may occur for $Z < 0$, extraction of both D and Z from experimental
9 transients is best undertaken through full simulation of the waveshape, with the parameter

10
11
12
13
14 $Z + \lg \frac{K_p}{\sqrt{\Lambda_f}}$ enabling iterative optimisation of experimental and simulated transients.
15
16
17

18 Having thus investigated the various parameters within our regular solution theory model, we
19 next re-examine the experimental data illustrated in Figure 1d.
20
21
22

23 *Analysis of the Experimental Data in Figure 1d.*

24
25 The two experimental permeation curves depicted in Figure 1d correspond to the CO_2 flux in
26 the polymers PVDF and PA66. In the former polymer film, the permeation flux is considered
27 to gradually increase with time, whilst in the latter membrane, a flux maximum is apparent
28 close to 50 h. The regular solution model developed would suggest slow transport in the
29 acceptor compartment, with repulsive interactions (*q.v.* Figure 5a for $Z < 0$). However,
30 consideration of the experimental equipment in Supplementary Information S1 (which is
31 analogous to that reported in reference 35) would indicate that the boundary condition $q = 0$
32 at $x = b$ is upheld. This apparent paradox suggests that an alternative explanation exists for
33 the permeation flux waveshape: the increase in the diffusion coefficient within PVDF may be
34 caused by the plasticisation of the polymer by supercritical CO_2 , which results in an increase
35 in its free volume and a decrease in its glass transition temperature; in contrast, the
36 supercritical CO_2 may extract the plasticiser in PA66, which results in a decrease in free
37 volume and hence a decrease in the diffusion coefficient. In any case, these insights stress the
38 importance of characterising chemical and physical effects during permeation processes.
39
40
41
42
43
44
45
46
47
48
49
50
51
52
53
54
55
56
57
58
59
60

Conclusions

In this work, we have sought to unravel the physicochemical whys and wherefores underpinning the observation of non-classical permeation transients, using regular solution theory to account for non-ideal permeant activity coefficients within a membrane. Accordingly, we have sought to develop protocols for experimental scientists and engineers to treat such data, thereby measuring, in a self-consistent manner, the ideal diffusion coefficient of a permeant through the membrane and its permeability. We have demonstrated that both classical and non-classical signals may be observed under specific conditions based on interactions with the polymer membrane and abnormal waveshapes cannot be merely denoted as pertaining to membrane swelling, as seemingly suggested within the literature.³⁸ Moreover, we have identified that even the classical, sigmoidal-shaped transient may not be interpreted simplistically, as *both* its steady-state limiting flux *and* its half-limiting time are affected by the membrane kinetics and nature and degree of molecular interaction between the permeating species and the membrane. This, in itself, strongly encourages a re-examination of existing steady-state permeation flux transient data sets, centred with a goal to identify *self-consistent* Fickian diffusion coefficients of the permeants within the membranes. In returning to the non-classical waveshapes identified in Figure 1, we conclude that peaks are only observed in first flood permeation flux transients when either no interactions or attractive interactions (*viz.*, those for which the activity coefficient is at most unity) occur between the permeating species and the membrane, *and* when either the transfer kinetics are slow and unfavourable at the membrane | acceptor cell interface, or transport in the acceptor compartment is slow. In contrast, split permeation flux transient waves occur when there is a repulsive interaction between the permeating species and the membrane (*viz.*, the permeant activity coefficient is greater than unity in the membrane) and when either the mass transport within the acceptor cell is slow, or when the permeant transfer rate across the membrane | acceptor interface is slow compared with permeation within the membrane. An interesting aspect of this work is the determination of the polymer-permeant interaction parameter Z from experimental diffusion measurements using either ψ_{lim} or τ_{50} , and this encourages further work to validate this approach to measure Z and compare it with the Flory-Huggins interaction parameter χ (equation 15), often measured using inverse gas chromatography.³⁹ This toolkit for experimentalists can assess the validity of diffusion measurements and also extract the interaction parameters.

In taking this forward, it is important to enquire as to whether a flux transient may provide information on the chemical degradation of a membrane. In answering this question, the combination of membrane thickness and mass measurements together with a series of double-step permeation processes – make way for accelerated permeation tests over single permeation measurements.

Acknowledgements

BC thanks TWI, Ltd. for financial support; SMK, NSL and JDW thank The University of Hull for support. We thank Barnaby E. King (TWI) for undertaking the permeation transients reported in Figure 1d. Some of the codes within this work were developed with financial support from EPSRC (GR/N EP/G020833/1). We thank one of the reviewers of this manuscript for assisting us in developing the comparison between our regular solution model and Flory-Huggins theory (equations (9)-(15)), and for insightful comments relevant to our experimental work.

Supporting Information

Description of the experimental methods

Effect of diffusion coefficients on flux transients

Effect of interfacial kinetics on flux transients

References

References and Notes

1. See, for example, Baker, R. W. (ed.), *Membrane Technology and Applications*, 2nd Edn., John Wiley, Chichester, 2004.
2. (a) Fernando, U. S.; Sheldrake, T.; Davidson, M., Critical assessment of PVDF multilayer barriers in unbounded flexible risers: applications and benefits, *Proceedings of the 32nd ASME International Conference on Ocean, Offshore and Arctic Engineering*, **2013**, OMAE2013-11237, VD4BT04A035; (b) Taravel-Condât, C.; Epsztein, T., The use of flexible pipe for CO₂-enhanced oil recovery applications, *Proceedings of the 31st ASME International Conference on Ocean, Offshore and Arctic Engineering*, **2012**, OMAE2012-83321, 251; (c) Rubin, A.; Wang, C., Qualification of flexible dynamic risers for supercritical CO₂, *Offshore Technology Conference*, **2012**, OTC-23339-MS, April 30 – May 3, Houston, Texas, USA.
3. Suleman, M. S.; Lau, K. K.; Yeong, Y. F., Plasticization and swelling in polymeric membranes in CO₂ removal from natural gas, *Chem. Eng. Technol.*, **2016**, *39*, 1604.
4. Sarrasin, F.; Memari, P.; Klopffer, M. H.; Lachet, V.; Taravel-Condât, C.; Rousseau, B.; Espuche, E., Influence of high pressures on CH₄, CO₂ and H₂S solubility in polyethylene: experimental and molecular simulation approaches for pure gas and gas mixtures: modelling of the sorption isotherms, *J. Memb. Sci.*, **2015**, *490*, 380.
5. (a) Wright J., The use of engineered polymers for the transport of hydrocarbons with high levels of CO₂, H₂S and brine to eliminate corrosion experienced with steel pipe lines in the oilfield, Rapra, *High Performance Polymers for Oil and Gas Conference Proceedings*, **2013**; (b) Schmitz J, High Density Polyethylene Liners for High Temperature and Gaseous Applications, *Conference Proceedings for Corrosion 13th Middle East*, **2010**, Paper No 10073; (c) Brogden S.; Fryer M., The effectiveness of polymer lined pipelines for subsea water injection service, *Conference Proceedings for MERL Oilfield Engineering with Polymers*, London, **2010**; (d) Hall S. J., Hill D. J.; Dang P., Plastic liners for hydrocarbon transport: A qualified and cost efficient alternative to CRAs, *OTC-19937*, **2009**.
6. Baptista, A.; Pinho, C.; Pinto, G.; Ribeiro, L.; Monteiro, J.; Santos, T. Assessment of an Innovative Way to Store Hydrogen in Vehicles, *Energies*, **2019**, *12*, 1762.
7. Gondal, I. A., Hydrogen integration in power-to-gas networks, *Int. J. Hydrogen Energy*, **2019**, *44*, 1803.
8. Graber, L., Improving the Accuracy of SF₆ Leakage Detection for High Voltage Switchgear. *IEEE Trans. Dielect. Electr. In.* **2011**, *18*, 1835.
9. (a) Binks, B. P.; Fletcher, P. D. I.; Johnson, A. J.; Elliott, R. P., How membrane permeation is affected by donor delivery solvent, *Phys. Chem. Chem. Phys.*, **2012**, *14*, 15525; (b) *Idem.*, Membrane permeation of testosterone from either solutions, particle dispersions or particle-stabilised emulsions, *Langmuir*, **2012**, *28*, 2510.
10. See, for example, Peighambaroust, S. J.; Rowshanzamir, S.; Amjadi, M., Review of the proton exchange membranes for fuel cell applications, *Int. J. Hydrogen Energy*, **2010**, *35*, 9349.
11. (a) Chandrasekaran, S. K.; Michaels, A. S.; Campbell, P. S.; Shaw, J. E., Scopolamine permeation through human skin *in vitro*, *A. I. Ch. E. Journal*, **1976**, *22*, 828; (b) Kubota, K.; Twizell, E. H., A non-linear numerical model of percutaneous drug absorption, *Math. Biosci.*, **1992**, *108*, 157.
12. (a) Mao, F.; Ong, S. K.; Gaunt, J. A., Modelling benzene permeation through drinking water high density polyethylene (HDPE) pipes, *J. Water Health*, **2015**, *13*, 758; (b) Hobson, A. J.; Stewart, D. I.; Bray, A. W.; Mortimer, R. J. G.; Mayes, W. M.; Riley, A. L.; Rogerson, M.; Burke, I. T., Behaviour and fate of vanadium during the aerobic neutralisation of hyperalkaline slag leachate, *Sci. Tot. Environ.*, **2018**, *643*, 1191.
13. Kujawski, W., Application of pervaporation and vapour permeation in environmental protection, *Polish J. Environ. Stud.*, **2000**, *9*, 13.
14. (a) See, for example Murer, P, *La Transition Énergétique*, Editions Mille et une nuits, Fayard, Paris, 2014; (b) Ropital, F, *Corrosion et Dégradation des Matériaux Métalliques*, IFP Publications, Editions Technip, Paris, 2009; (c) Cheng, Y. F., *Stress Cracking Corrosion of Pipelines*, John Wiley, Hoboken, New Jersey, 2013; (d) Standard methods for evaluating hydrogen permeation through metals are given in the ASTM G148-97(2018) and ISO 17081:2014 protocols.
15. (a) Crank, J., *The Mathematics of Diffusion*, 2nd Edn., Oxford University Press, Oxford, 1975; Barrer, R. M.; Rideal, E. K., Permeation, diffusion and solution of gases in organic polymers, *Trans. Faraday Soc.*, **1939**, *35*, 628.
16. Heilman, W; Tammela, V; Meyer, J. A; Stannett, V; Szwarc, M., Permeability of Polymer Films to Hydrogen sulfide Gas. *J. Ind. Eng. Chem.* **1956**, *48*, 821.
17. Hsu, K. H., A diffusion model with a concentration-dependent diffusion coefficient for describing water movement in legumes during soaking, *J. Food Sci.*, **1983**, *48*, 618.
18. (a) Islam, M. A.; Buschatz, H.; Paul, D., Non-equilibrium surface reactions – a factor in determining steady-state diffusion flux, *J. Memb. Sci.*, **2002**, *204*, 379; (b) Rim, J. E.; Pinsky, P. M.; van Osdol, W. W., Finite element modelling of coupled diffusion with partitioning in transdermal drug delivery, *Ann. Biomed. Eng.*, **2005**, *33*, 1422.
19. Shieh, J.-J; Huang, R. Y. M., A pseudophase-change solution-diffusion model for pervaporation II: binary mixture permeation, *Sep. Sci. Technol.*, **1998**, *33*, 933.
20. Edwards, D. A., Non-Fickian diffusion in thin polymer films, *J. Polym. Sci. B, Polym. Phys.*, **1996**, *34*, 981.
21. Nestle, N. F. E. I.; Kimmich, R., Concentration-dependent diffusion coefficients and sorption isotherms: application to ion exchange processes as an example, *J. Phys. Chem.*, **1996**, *100*, 12569.
22. Kokes, R. J.; Long, F. A., Diffusion of organic vapours into polyvinyl acetate, *J. Am. Chem. Soc.*, **1953**, *75*, 6142.
23. Frisch, H. L., The time lag in diffusion, *J. Phys. Chem.*, **1957**, *61*, 93.
24. *Idem.*, Sorption and transport in glassy polymers: a review, *Polym. Eng. Sci.*, **1980**, *20*, 2.
25. Karimi, M., Diffusion in polymer solids and solutions, in Markoi, J., *Mass Transfer in Chemical Engineering Processes*, InTech, Rijeka, Croatia, 2011.
26. Stern, S. A.; Frisch, H. L., The selective permeation of gases through polymers, *Ann. Rev. Mater. Res.*, **1981**, *11*, 523.

- 1
2
3
4
5
6
7
8
9
10
11
12
13
14
15
16
17
18
19
20
21
22
23
24
25
26
27
28
29
30
31
32
33
34
35
36
37
38
39
40
41
42
43
44
45
46
47
48
49
50
51
52
53
54
55
56
57
58
59
60
27. Srinivasan, R.; Auvil, S. R.; Burbán, P. M., Elucidating the mechanism(s) of gas transport in poly[1-(trimethylsilyl)-1-propyne] (PTMSP) membranes, *J. Memb. Sci.*, **1994**, *86*, 67.
 28. Masaro, L.; Zhu, X. X., Physical models of diffusion for polymer solutions, gels and solids, *Prog. Polym. Sci.*, **1999**, *24*, 731.
 29. Reynier, A.; Dole, P.; Humbel, S.; Feigenbaum, A., Diffusion coefficients of additives in polymers I: correlation with geometric parameters, *J. Appl. Polym. Sci.*, **2001**, *82*, 2422.
 30. Flaconnèche, B.; Martin, J.; Klopffer, M. H., Transport properties of gases in polymers: experimental methods, *Oil Gas Sci. Technol. – Rev. IFP*, **2001**, *56*, 245.
 31. Fakirov, S.; Krasteva, B., On the glass transition temperature of polyethylene as revealed by micro-hardness measurements, *J. Macromolec. Sci. B*, **2000**, *39*, 297.
 32. Park, J. K.; Nibras, M., Mass flux of organic chemicals through polyethylene geomembranes, *Water Environ. Res.*, **1993**, *65*, 227.
 33. Firpo, G.; Angeli, E.; Repetto, L.; Valbusa, U., Permeability thickness dependence of polydimethylsiloxane (PDMS) membranes, *J. Memb. Sci.*, **2015**, *481*, 1.
 34. Berean, K.; Ou, J. Z.; Nour, M.; Latham, K.; McSweeney, C.; Paull, D.; Halim, A.; Kentish, S.; Doherty, C. M.; Hill, A. J.; Kalantar-Zadeh, K., The effect of cross-linking temperature on the permeability of PDMS membranes: evidence of extraordinary CO₂ and CH₄ gas permeation, *Sep. Pur. Technol.*, **2014**, *122*, 96.
 35. Craster, B.; Jones, T. G. J., Permeation of a range of species through polymer layers under varying conditions of temperature and pressure: *in situ* measurement methods, *Polymers*, **2019**, *11*, 1056.
 36. Cussler, E., *Diffusion: Mass Transfer in Fluid Systems*, 3rd Edn., Cambridge University Press, Cambridge, 2009.
 37. (a) See, for example, McClelland, B. J., *Statistical Thermodynamics*, Chapman and Hall, London, 1973; (b) Hagen, T. A.; Flynn, G. L., Permeation of hydrocortisone and hydrocortisone 21-alkyl esters through silicone rubber membranes: relationship to regular solution solubility behaviour, *J. Memb. Sci.*, **1987**, *30*, 47; (c) Compton, R. G.; Laing, M. E.; Ledwith, A.; Abu-Abdoun, I. I., Polymer-coated electrodes: cyclic voltammetry and chronoamperometry of non-ideal systems – the anodic oxidation of poly(4-vinyl-triphenylamine) films, *J. Appl. Electrochem.*, **1988**, *18*, 431; (d) Ball, J. C.; Marken, F.; Fulian, Q.; Wadhawan, J. D.; Blythe, A. N.; Schröder, U.; Compton, R. G.; Bull, S. D.; Davies, S. G., Voltammetry of electroactive oil droplets: Part II: Comparison of experimental and simulated data for coupled ion and electron insertion processes and evidence for microscale convection, *Electroanalysis*, **2000**, *12*, 1017; (e) Scovazzo, P.; Camper, D.; Kieft, J.; Poshusta, J.; Koval, C.; Noble, R., Regular solution theory and CO₂ gas solubility in room-temperature ionic liquids, *Ind. Eng. Chem. Res.*, **2004**, *43*, 6855; (f) Corbyn, C. P.; Fletcher, P. D. I.; Gemici, R.; Dias, R. S.; Miguel, M. G., Re-dissolution and de-compaction of DNA-cationic surfactant complexes using non-ionic surfactants, *Phys. Chem. Chem. Phys.*, **2009**, *11*, 11568; (g) Halls, J. E.; Altalhi, A. A.; de Abreu, F. C.; Goulart, M. O. F. G.; Wadhawan, J. D., Concentration-dependent diffusion coefficients of *tert*-butylferrocene within didodecyltrimethylammonium chloride/brine liquid crystals, *Electrochem. Commun.*, **2012**, *17*, 41.
 38. (a) Poling, B. E.; Prausnitz, J. M.; O'Connell, J. P., *The Properties of Gases and Liquids*, 5th edn., McGraw-Hill, New York, 2001, pp.843-4; (b) Volume changes in the membrane due to the take up of permeant molecules in the framework of compressible regular solution theory have been described in reference 38(c) and (d); (b) Rezakazemi, M.; Shirazian, S., Gas permeation prediction through polymeric membranes using compressible regular solution theory, *Int. J. Hydrogen Energy*, **2018**, *43*, 22357; (c) Merkel, T. C.; Bondar, V. I.; Nagai, K.; Freeman, B. D.; Pinnau, I., Gas sorption, diffusion and permeation in poly(dimethylsiloxane), *J. Polymer Sci. B: Polymer Phys.*, **2000**, *38*, 415; (e) Zielinski, J. M.; Duda, J. L., Predicting polymer/solvent diffusion coefficients using free-volume theory, *AIChE J.*, **1992**, *38*, 405.
 39. Tian, M.; Munk, P., Characterisation of polymer-solvent interactions and their temperature dependence using inverse gas chromatography, *J. Chem. Eng. Data*, **1994**, *39*, 742.
 40. Peerce, P. J.; Bard, A. J., Polymer films on electrodes: Part II: Film structure and mechanism of electron transfer within electrodeposited poly(vinylferrocene), *J. Electroanal. Chem.*, **1980**, *112*, 97.
 41. Savéant, J.-M., Permeation through polymer coatings on electrodes: membrane *versus* pinhole permeation, *J. Electroanal. Chem.*, **1991**, *302*, 91.
 42. Amatore, C.; Szunerits, S.; Thouin, L.; Warkocz, J.-S., The real meaning of Nernst's steady diffusion layer concept under non-forced hydrodynamic conditions: a simple model based on Levich's seminal view of convection, *J. Electroanal. Chem.*, **2001**, *500*, 62.
 43. (a) Halls, J. E.; Wadhawan, J. D., A model for efficient, semiconductor-free solar cells *via* supersensitized electron transfer cascades in photogalvanic devices, *Phys. Chem. Chem. Phys.*, **2013**, *15*, 3218; (b) Halls, J. E.; Hawthornthwaite, A.; Hepworth, R. J.; Roberts, N. A.; Wright, K. J.; Zhou, Y.; Haswell, S. J.; Haywood, S. K.; Kelly, S. M.; Lawrence, N. S.; Wadhawan, J. D., Empowering the smart grid: can redox batteries be matched to renewable energy systems for energy storage? *Energy Environ. Sci.*, **2013**, *6*, 1026.
 44. Copies of the programs used are available from the authors, upon request.

Table 1: Variation of the dimensionless limiting flux (ψ_{lim}) and time required to reach 50% of the steady flux (τ_{50}) value as a function of the interaction parameter, Z for membrane-limiting transport, with fast (reversible) partition kinetics at the membrane | acceptor phase boundary. Data obtained through cubic-spline interpolation from simulated transients. Simulations used a 0.2 mm thick membrane and lasted for 100 s, with $c_o = 1.0$ mM, with membrane diffusion coefficient at infinite dilute, $D = 10^{-9}$ m² s⁻¹ with fast transport in the acceptor phase ($D_p = 1.5 \times 10^{-4}$ m² s⁻¹), with $K_p = 1.0$, $k_f = k_b = 1.0$ m s⁻¹.

Z	Ψ_{lim}	τ_{50}
-1.5	1.50	0.979
-1.0	1.33	1.08
-0.5	1.17	1.21
0.0	1.00	1.37
+0.5	0.833	1.57
+1.0	0.667	1.83
+1.5	0.500	2.14

Table 2: Variation of the dimensionless limiting flux ($\psi_{lim/\vartheta}$) and time required to reach 50% of the steady flux (τ_{50}) value as a function of the interaction parameter, Z for membrane-limiting transport, with variable kinetics at the membrane | acceptor phase boundary. Data obtained through cubic-spline interpolation from simulated transients. Simulations used a 0.2 mm thick membrane and lasted for 100 s, with $c_o = 1.0$ mM, with membrane diffusion coefficient at infinite dilute, $D = 10^{-9}$ m² s⁻¹ with fast transport in the acceptor phase ($D_p = 1.5 \times 10^{-4}$ m² s⁻¹).

		Z = -1.5		Z = -1.0		Z = -0.5		Z = 0.0		Z = 0.5		Z = 1.0		Z = 1.5	
lgΛ_f	lgK_P	Ψ_{ϑ}	τ_{ϑ}												
5.5	0	1.50	0.979	1.33	1.08	1.17	1.21	1.00	1.37	0.833	1.57	0.667	1.83	0.500	2.14
5.5	2	1.50	0.979	1.33	1.08	1.17	1.21	1.00	1.37	0.833	1.57	0.667	1.83	0.500	2.14
5.5	4	1.50	0.979	1.33	1.08	1.17	1.21	1.00	1.37	0.833	1.57	0.667	1.83	0.500	2.14
5.5	6	1.50	0.979	1.33	1.08	1.17	1.21	1.0	1.37	0.833	1.57	0.667	1.83	0.500	2.14
3.5	-2	1.50	0.988	1.33	1.09	1.17	1.22	0.996	1.38	0.830	1.59	0.664	1.84	0.498	2.16
3.5	0	1.50	0.980	1.33	1.09	1.17	1.21	0.999	1.37	0.833	1.57	0.666	1.83	0.500	2.14
3.5	2	1.50	0.980	1.33	1.09	1.17	1.21	0.999	1.37	0.833	1.57	0.666	1.83	0.500	2.14
3.5	4	1.50	0.980	1.33	1.09	1.17	1.21	1.00	1.37	0.833	1.57	0.666	1.83	0.500	2.14
1.5	-4	0.909	1.50	0.845	1.67	0.773	1.88	0.690	2.15	0.595	2.51	0.488	2.98	0.369	3.57
1.5	-2	1.42	1.08	1.26	1.19	1.11	1.33	0.949	1.51	0.792	1.73	0.634	2.01	0.475	2.35
1.5	0	1.42	1.07	1.27	1.19	1.11	1.33	0.952	1.50	0.794	1.72	0.636	2.00	0.477	2.34
1.5	2	1.42	1.07	1.27	1.19	1.11	1.33	0.952	1.50	0.794	1.72	0.636	2.00	0.477	2.34
-0.5	-6	0.0217	2.34	0.0217	2.66	0.0217	3.09	0.0217	3.68	0.0217	4.56	0.0216	6.01	0.0213	8.90
-0.5	-4	0.160	2.14	0.159	2.43	0.158	2.83	0.156	3.38	0.154	4.22	0.151	5.66	0.144*	8.72*
-0.5	-2	0.171	2.21	0.170	2.42	0.168	2.81	0.166	3.36	0.164	4.19	0.160	5.62	0.152*	8.66*
-0.5	0	0.171	2.12	0.170	2.42	0.168	2.81	0.166	3.36	0.164	4.19	0.160	5.62	0.152*	8.66*

*Permeation transient waveshape comprises a “split-wave” (see text).

1
2
3
4
5
6
7
8
9
10
11
12
13
14
15
16
17
18
19
20
21
22
23
24
25
26
27
28
29
30
31
32
33
34
35
36
37
38
39
40
41
42
43
44
45
46

Table 3: Equations describing the variation of the characteristic parameters of a permeation flux transient ($\psi_{lim/\vartheta}$ and τ_{50}) with interaction parameter Z within the framework of the limiting behaviour regions provided by the kinetic zone diagram illustrated in Figure 6c. For each expression given, the square of the correlation coefficient, R^2 , is provided in parentheses.

Region	Ψ_{ϑ}	τ_{50}
Pure diffusion (PD) ^a	$\psi_{\vartheta} = 1 - \frac{1}{3}Z$ ($R^2 = 1$)	$\tau_{50} = 1.41e^{0.260Z}$ ($R^2 = 0.994$)
Equilibrium diffusion (ED) ^b	$\psi_{\vartheta} = 0.998 - 0.332Z$ ($R^2 = 1$)	$\tau_{50} = 1.41e^{0.260Z}$ ($R^2 = 0.994$)
General kinetics (GK) ^c	$\psi_{\vartheta} = 0.951 - 0.315Z$ ($R^2 = 1.00$)	$\tau_{50} = 1.54e^{0.260Z}$ ($R^2 = 0.994$)
Quasi-Reversible Equilibrium (QRE) ^d	$\psi_{\vartheta} = 0.947 - 0.313Z$ ($R^2 = 1.00$)	$\tau_{50} = 1.54e^{0.260Z}$ ($R^2 = 0.994$)
	$\psi_{\vartheta} = 0.667 - 0.179Z$ ($R^2 = 0.988$)	$\tau_{50} = 2.23e^{0.289Z}$ ($R^2 = 0.991$)
Pure kinetics (PK) ^e	$\psi_{\vartheta} = f\left(Z + \lg \frac{K_p}{\sqrt{\Lambda_f}}\right)$	$\tau_{50} = f\left(Z + \lg \frac{K_p}{\sqrt{\Lambda_f}}\right)$

^aUncertainty less than 10⁻⁴% from equation (32).

^bUncertainty between 10⁻⁴ and 1% from equation (32).

^cUncertainty between 1 and 10% from equation (32).

^dTwo extreme sub-zones exist in this region, where uncertainty is between 10-60% from equation (32).

^eUncertainty greater than 60% from equation (32); split waveshapes appear for $Z = +1.5$.

Figure Legends

Figure 1

(a)

Ideal Fickian permeation flux transient at the membrane | acceptor cell interface. The acceptor compartment is considered as an infinite source and the permeant is sufficiently rapidly removed from the membrane in the acceptor cell. The transient was simulated using equation (3) with the following parameters. Concentration of permeant at the donor cell | membrane interface, $c_0 = 1.0$ mM; diffusion coefficient of permeant in the membrane, $D = 10^{-9}$ m² s⁻¹; membrane thickness, $b = 0.2$ mm; for the summation $n = 1000$ was used to approximate $n \rightarrow \infty$.

(b)

Permeation curves for a mixture comprising 80% methane (black) and 20% carbon dioxide (grey) through medium density polyethylene (MDPE) at 80 °C and 100 bar. *Reproduced with permission from Reference 30, Copyright © 2001, Éditions Technip.*

(c)

Sensor readings for methane (solid blue) and carbon dioxide (dashed orange) permeation through a cross-lined polydimethylsiloxane membrane at 30 °C in a liquid medium. *Reproduced with permission from Reference 34, Copyright © 2014, Elsevier.*

(d)

Carbon dioxide flux transients through a 1.0 mm thick PVDF (i), or PA66 (ii) membrane at 80 °C and 200 barg. Two types of permeation cell were used: large area (50.2655 cm², red and blue transients) and small area (12.5664 cm², magenta and black transients). The measured membrane thicknesses were PVDF (both permeation cells): 1.072 mm; PA66 large cell: 1.038 mm; PA66 small cell: 1.049 mm. See reference 35 and Supporting Information S1 for experimental details.

Figure 2

(a)

Schematic illustration of a constant pressure permeation cell, where a chemical species (the permeant) moves from a donor source through a membrane into an acceptor cell.

(b)

Concentration profiles for transport-limited permeation through a membrane based on the arrangement in panel (a), using equation (2) with the parameters: $c_0 = 1.0$ mM; $b = 0.2$ mm; $D = 10^{-9}$ m² s⁻¹. Note that the abscissa is presented as in a logarithmic scale. Transients were simulated at particular time snapshots in the range $10^{-5} \leq t/s \leq 10^5$, increasing as indicated by the arrow through one order of magnitude.

(c)

Ideal Fickian permeation flux transient at the membrane | acceptor cell interface. The acceptor compartment is considered as an infinite source and the permeant is sufficiently rapidly removed from the membrane in the acceptor cell. The transient was simulated using equation (3) with the following parameters. Concentration of permeant at the donor cell | membrane interface, $c_0 = 1.0$ mM; diffusion coefficient of permeant in the membrane, $D = 10^{-9}$ m² s⁻¹; membrane thickness, $b = 0.2$ mm; for the summation $n = 1000$ was used to approximate $n \rightarrow \infty$. The abscissa represents the logarithmic value of the dimensionless time (given by equation (18)), whilst the ordinate denotes the normalised flux (given by equation (23)), *vide infra*. This is the dimensionless equivalent of Figure 1(a).

(d)

Plot of the variation of the amount of permeant entering the acceptor cell per unit membrane area with time, illustrating the “time lag.” Graph simulated using equation (4), with the following parameters. Concentration of permeant at the donor cell | membrane interface, $c_0 = 1.0$ mM; diffusion coefficient of permeant in the membrane, $D = 10^{-9}$ m² s⁻¹; membrane thickness, $b = 0.2$ mm; for the summation $n = 1000$ was used to approximate $n \rightarrow \infty$. Note that the abscissa has a logarithmic scale.

Figure 3

Schematic illustration of the co-ordinate system and boundary conditions imposed within the model used within this work.

Figure 4

(a)

Simulated flux transients for membrane-limited permeation with fast (kinetically reversible) partition of permeant between the acceptor phase and the polymer membrane. Simulations used a 0.2 mm thick membrane and lasted for 100 s, with $c_0 = 1.0$ mM, with membrane diffusion coefficient at infinite dilute, $D = 10^{-9}$ m² s⁻¹ with fast transport in the acceptor phase ($D_p = 1.5 \times 10^{-4}$ m² s⁻¹), with $K_p = 1.0$, $k_f = k_b = 1.0$ m s⁻¹. Cyan circles refer to the classical permeation through a membrane simulated using equation (3); solid lines refer to flux transients simulated using regular solution theory, with interaction parameter $Z = -1.5$ (blue), -1.0 (green), -0.5 (red), 0 (cyan), 0.5 (magenta), 1.0 (gold), 1.5 (black).

(b)

Concentration profile of permeant within the membrane (of thickness b), normalised to the concentration of the infinite donor (c_0). Simulation parameters as for (a). Key: $Z = -1.5$ (blue, attractive polymer-permeant interactions), 0 (green, no polymer-permeant interactions), 1.5 (red, repulsive polymer-permeant interactions).

(c)

Concentration profile of emerging permeant from the membrane within the acceptor compartment. Simulation parameters as for (a); key as in panel (b).

(d)

Variation of the effective diffusion coefficient within the membrane. Simulation parameters as for (a); key as in panel (b).

(e)

Jackson diagram illustrating the algorithm for extracting the interaction parameter and self-consistent diffusion coefficient from experimental data under conditions of fast acceptor phase transport and fast kinetics at the membrane | acceptor phase boundary.

Figure 5

(a)

Permeation flux transients for the case of slow transport within the acceptor compartment; simulation parameters identical to those in Figure 4(a), with $D_p = 15D$. Key: interaction parameter $Z = -1.5$ (blue), -1.0 (green), -0.5 (red), 0 (cyan), 0.5 (magenta), 1.0 (gold), 1.5 (black).

(b)

Permeation flux transients as a function of the ratio of transport in the acceptor compartment to the membrane at infinite dilution (D_p/D) for $Z = -1.5$ (i), 0 (ii) and 1.5 (iii) with fast kinetics at the membrane | acceptor phase boundary, with $-3 \leq \lg \left\{ \frac{D_p}{D} \right\} \leq 5$. Supporting Information S2 illustrates figures for other values of the interaction parameter. All other simulation parameters are as for Figure 4(a).

(c)

Variation of the transport parameter, $\frac{\psi_g - \psi_{2g}}{\psi_g}$, with ratio of transport in the acceptor compartment to the membrane at infinite dilution (D_p/D). All other simulation parameters are as for Figure 4(a). Key: interaction parameter, $Z = -1.5$ (blue circles), -1.0 (green squares), -0.5 (red crosses), 0 (cyan pluses), 0.5 (magenta diamonds), 1.0 (gold triangles), 1.5 (black pentagons).

Figure 6

(a)

Permeation flux transients for the case of slow interfacial kinetics ($k_f = 0.01 \text{ m s}^{-1}$; $k_b = 1.00 \text{ m s}^{-1}$; $K_p = 0.01$) within the acceptor compartment; simulation parameters identical to those in Figure 4(a), with $D_p = 15D$. Key: interaction parameter $Z = -1.5$ (blue), -1.0 (green), -0.5 (red), 0 (cyan), 0.5 (magenta), 1.0 (gold), 1.5 (black).

(b)

Permeation flux transients as a function of the membrane | acceptor phase boundary partition coefficient, $K_p = \frac{k_f}{k_b}$, with $-0.5 \leq \lg K_p \leq 5.5$, for $Z = -1.5$ (i), 0 (ii) and 1.5 (iii) with variable kinetics at the membrane | acceptor phase boundary (see text). Supporting Information S3 illustrates figures for other values of the interaction parameter. All other simulation parameters are as for Figure 4(a).

(c)

Kinetic zone diagram illustrating the five regions controlled by kinetic and thermodynamic partition at the membrane | acceptor compartment interface. See text and Table 3 for the characteristics pertaining to each region.

Graphical Abstract

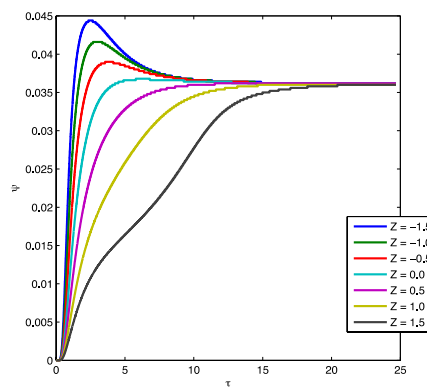
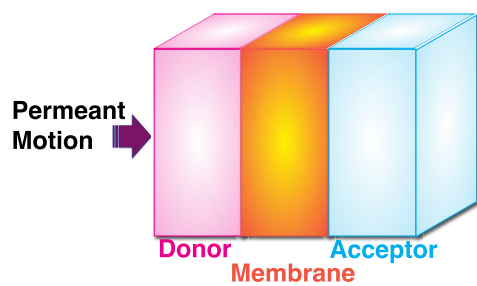


Figure 1a

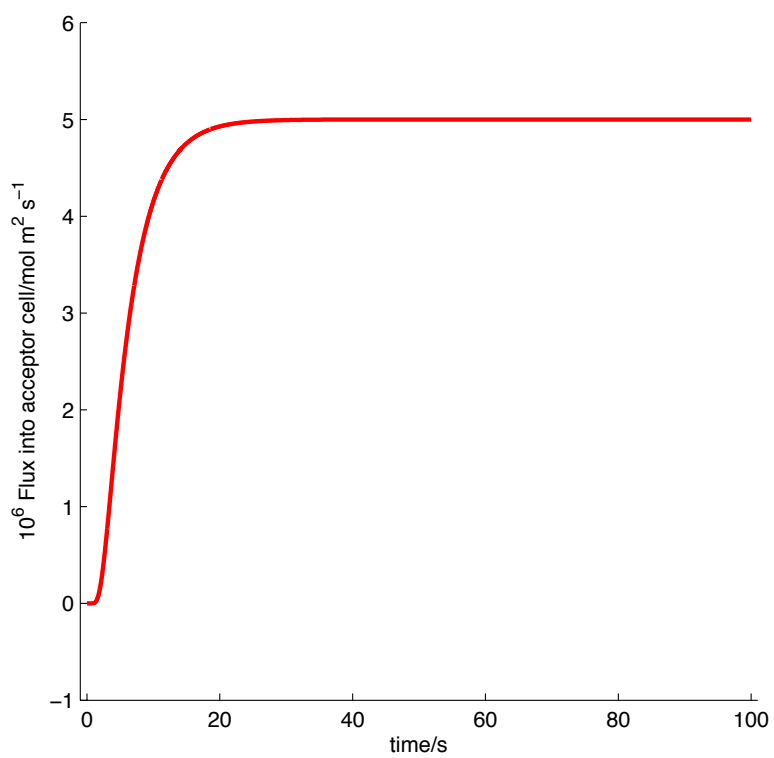


Figure 1b

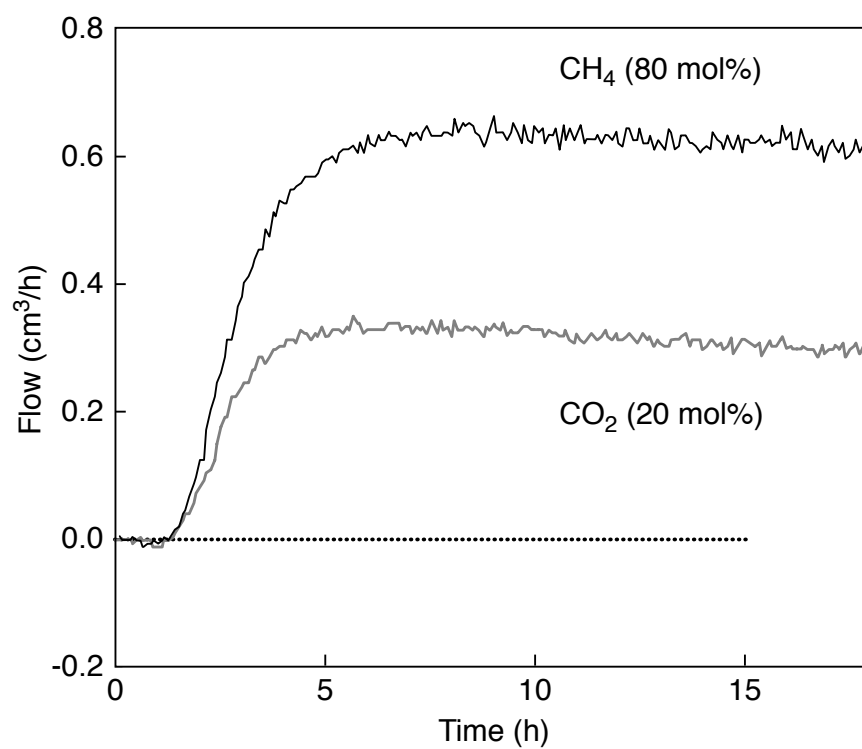


Figure 1c

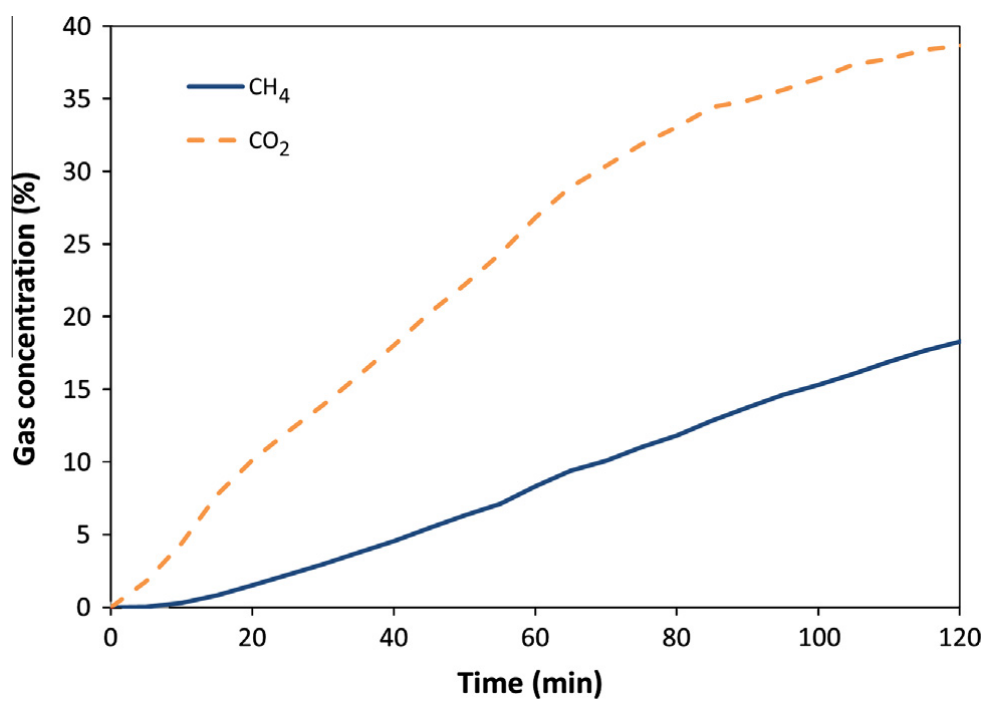


Figure 1d(i)

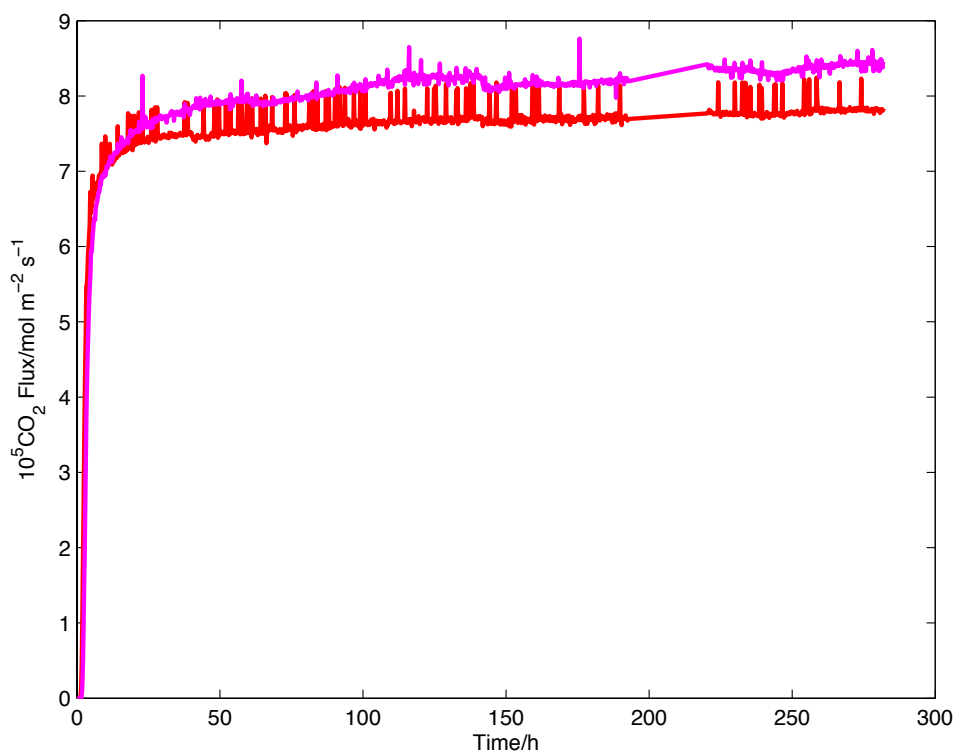


Figure 1d(ii)

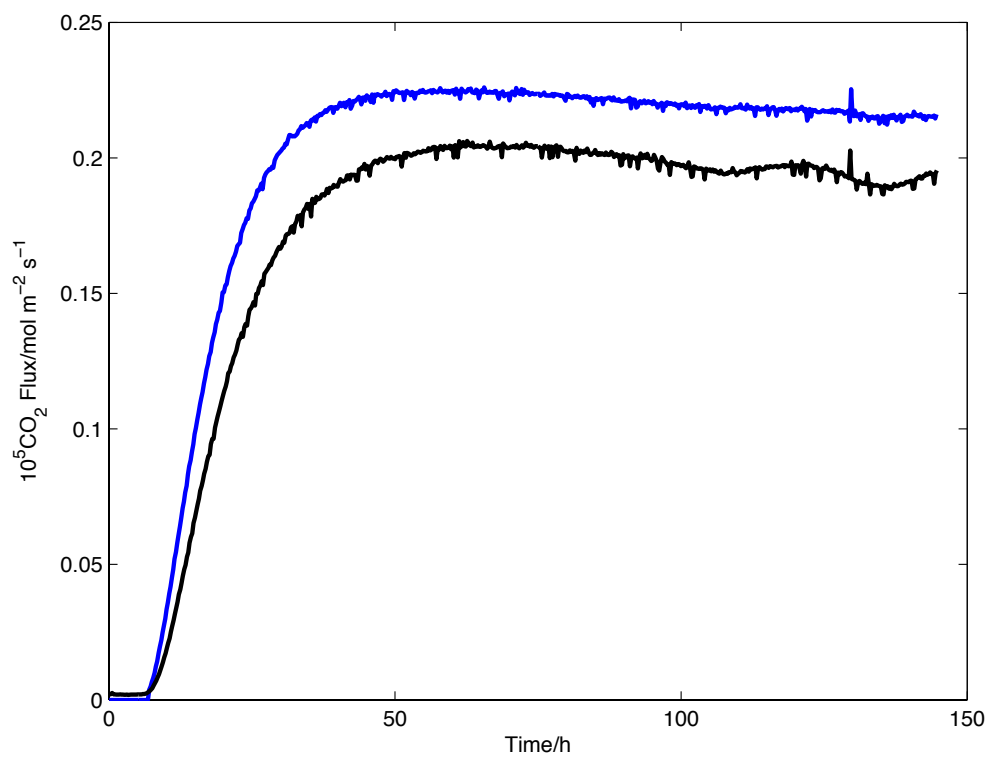


Figure 2a

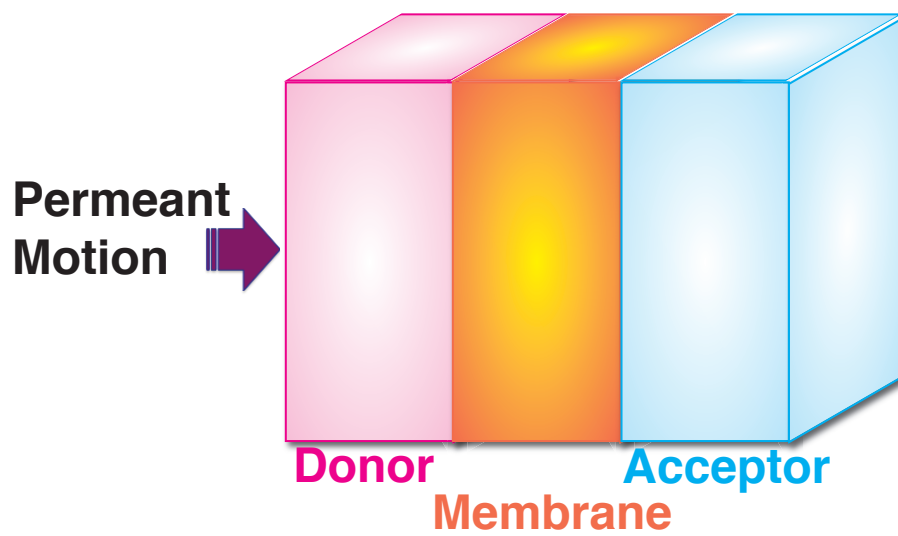
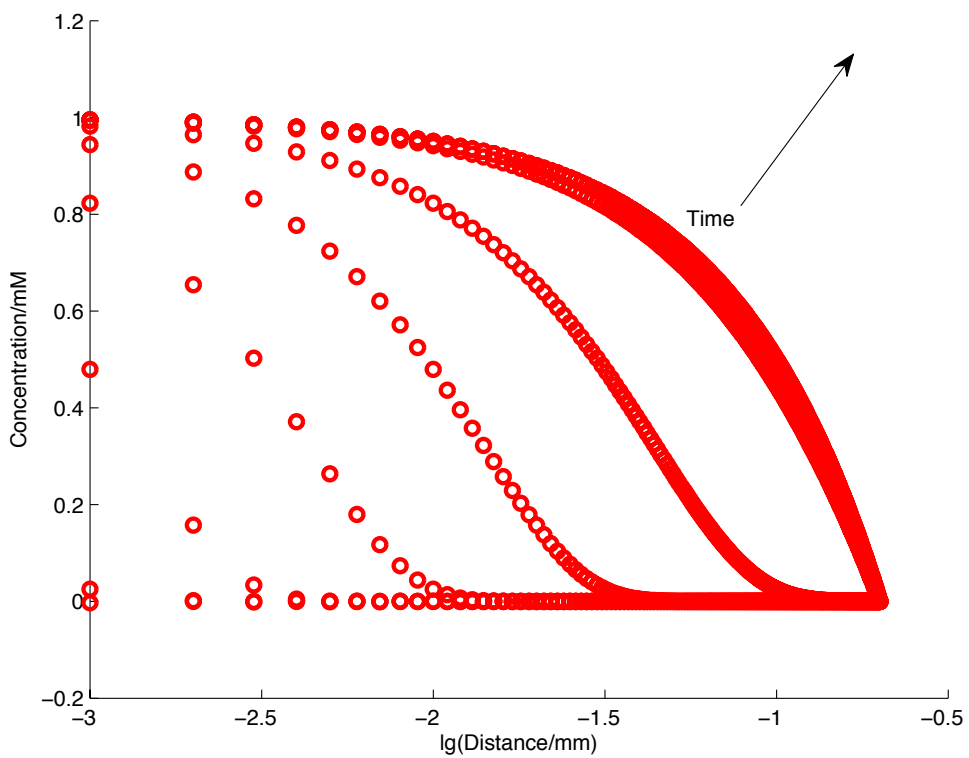


Figure 2b



1
2
3
4
5
6
7
8
9
10
11
12
13
14
15
16
17
18
19
20
21
22
23
24
25
26
27
28
29
30
31
32
33
34
35
36
37
38
39
40
41
42
43
44
45
46
47
48
49
50
51
52
53
54
55
56
57
58
59
60

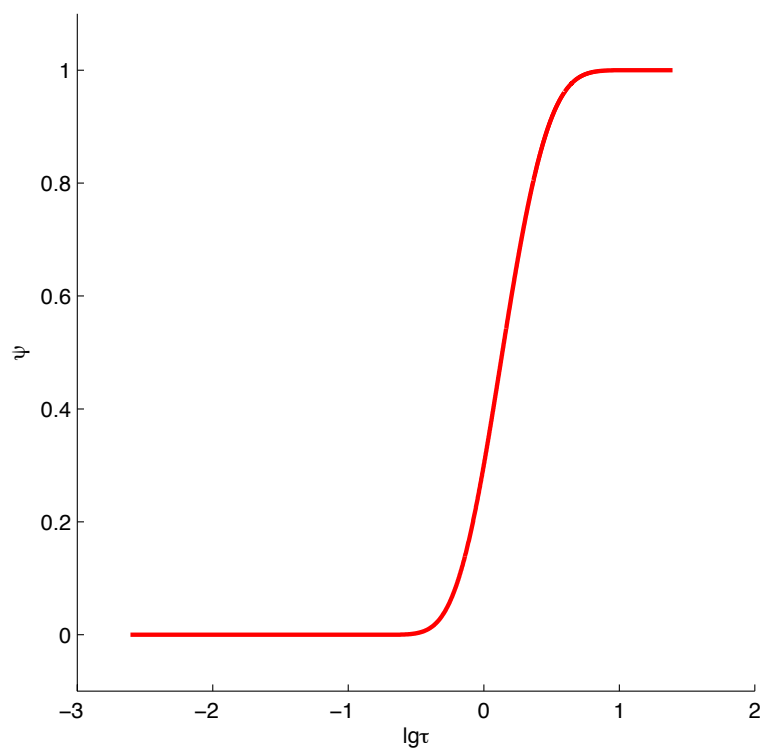
Figure 2c

Figure 2d

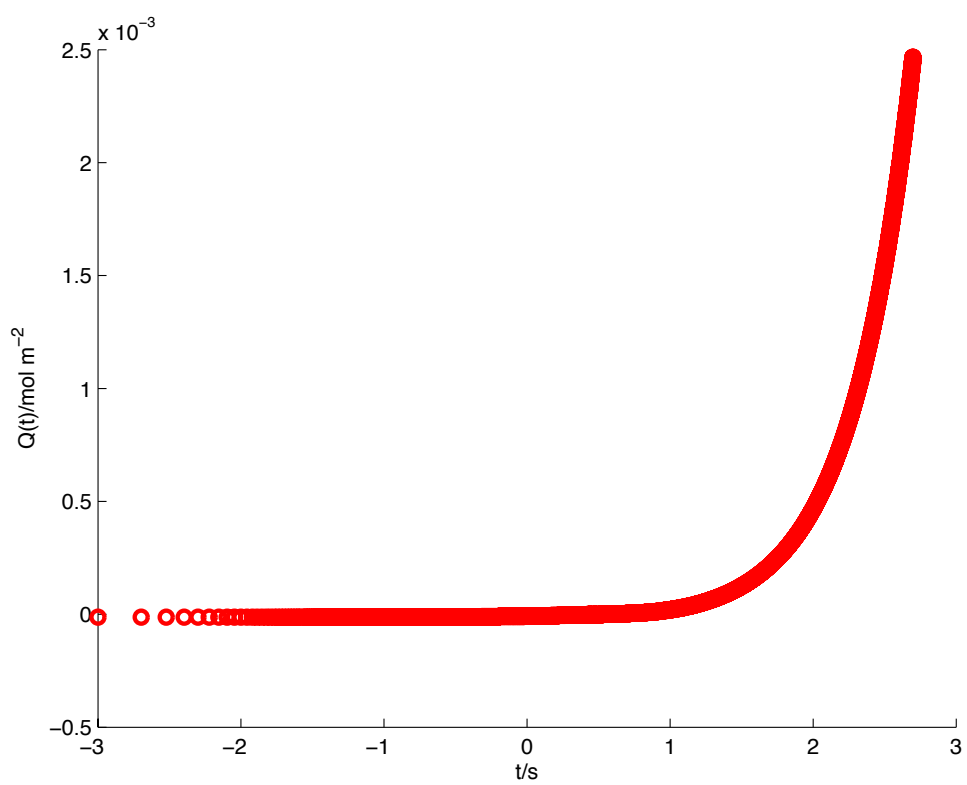


Figure 3

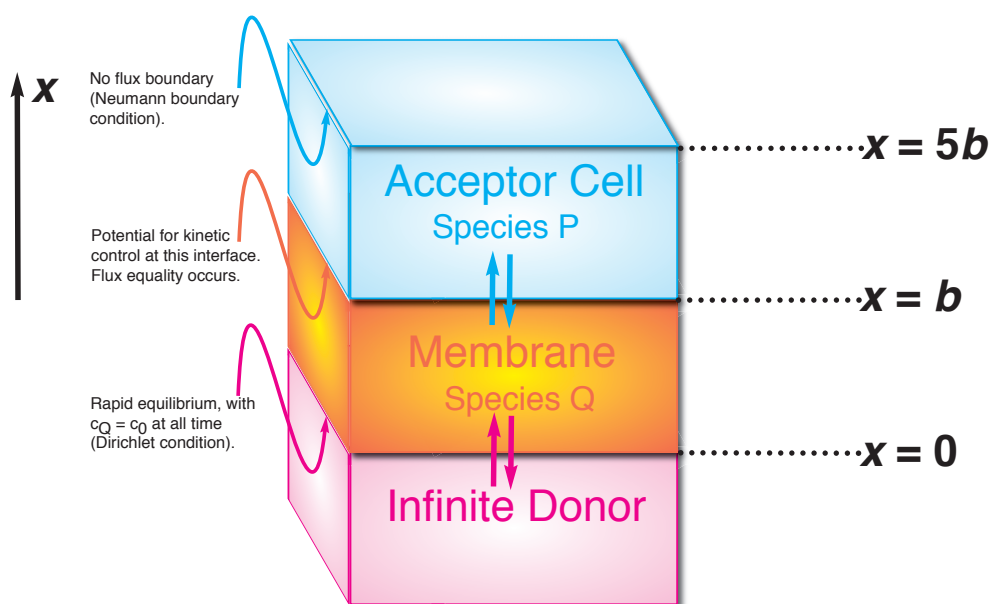


Figure 4a

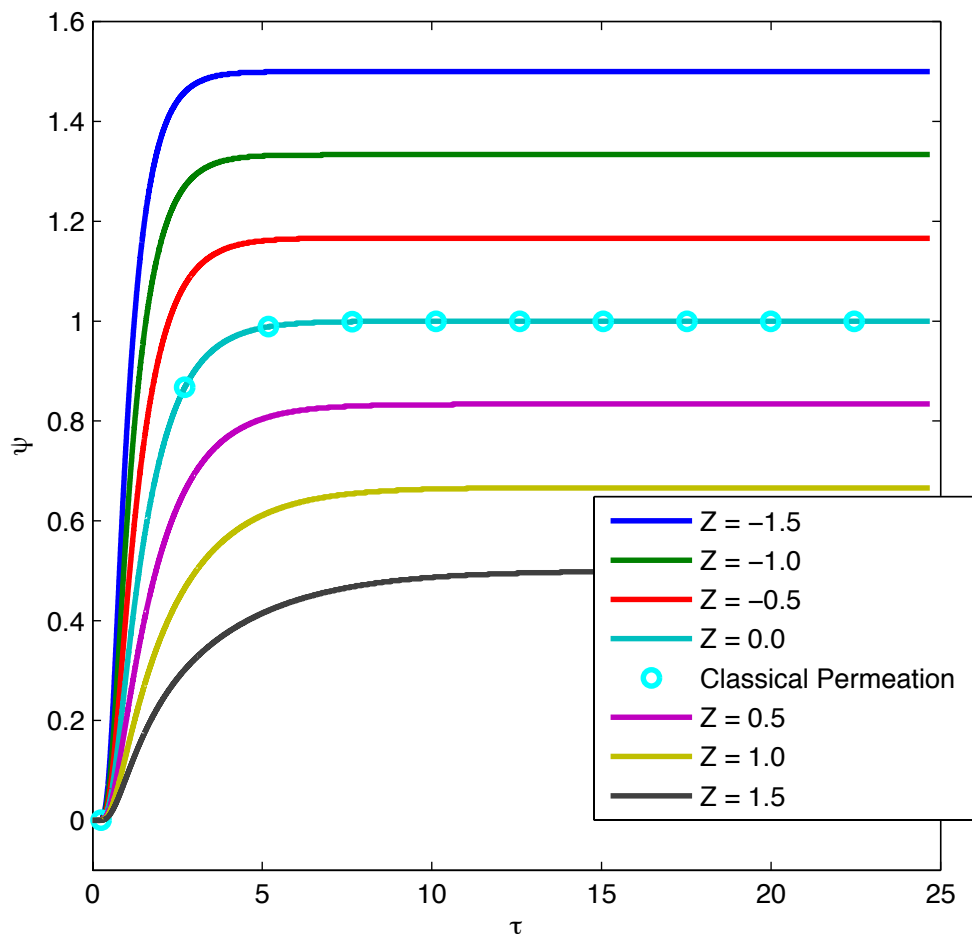


Figure 4b

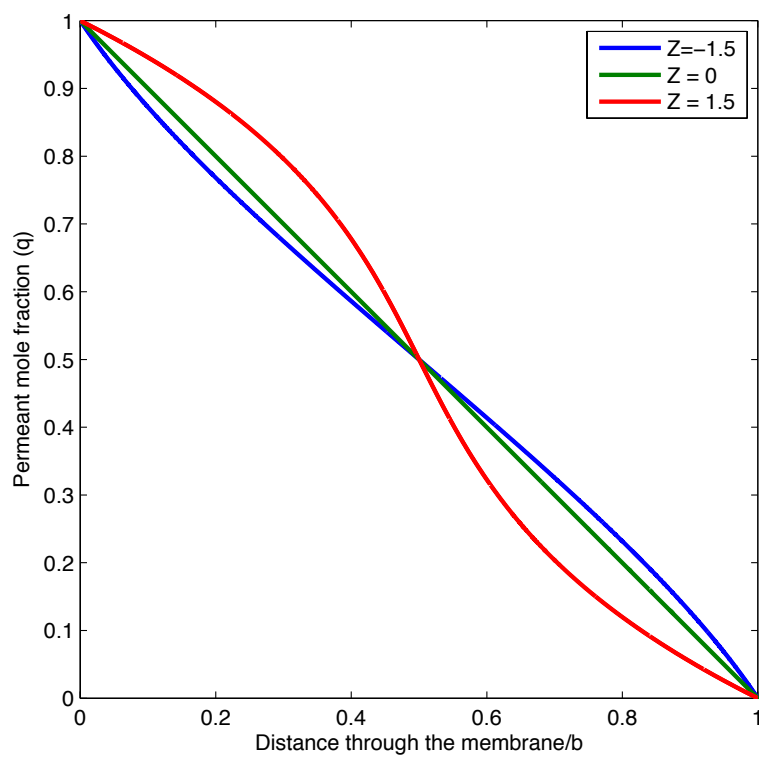
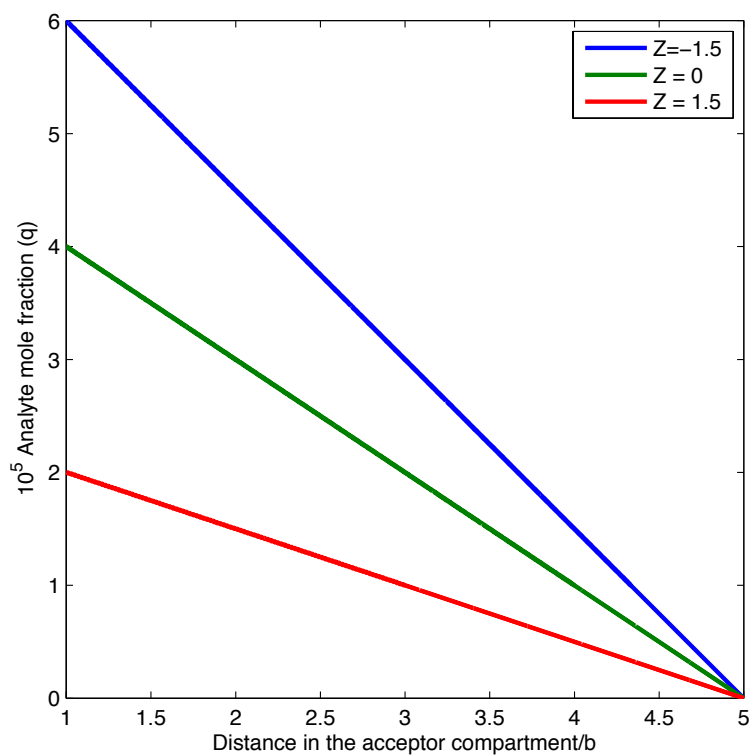


Figure 4c



1
2
3
4
5
6
7
8
9
10
11
12
13
14
15
16
17
18
19
20
21
22
23
24
25
26
27
28
29
30
31
32
33
34
35
36
37
38
39
40
41
42
43
44
45
46
47
48
49
50
51
52
53
54
55
56
57
58
59
60

Figure 4d

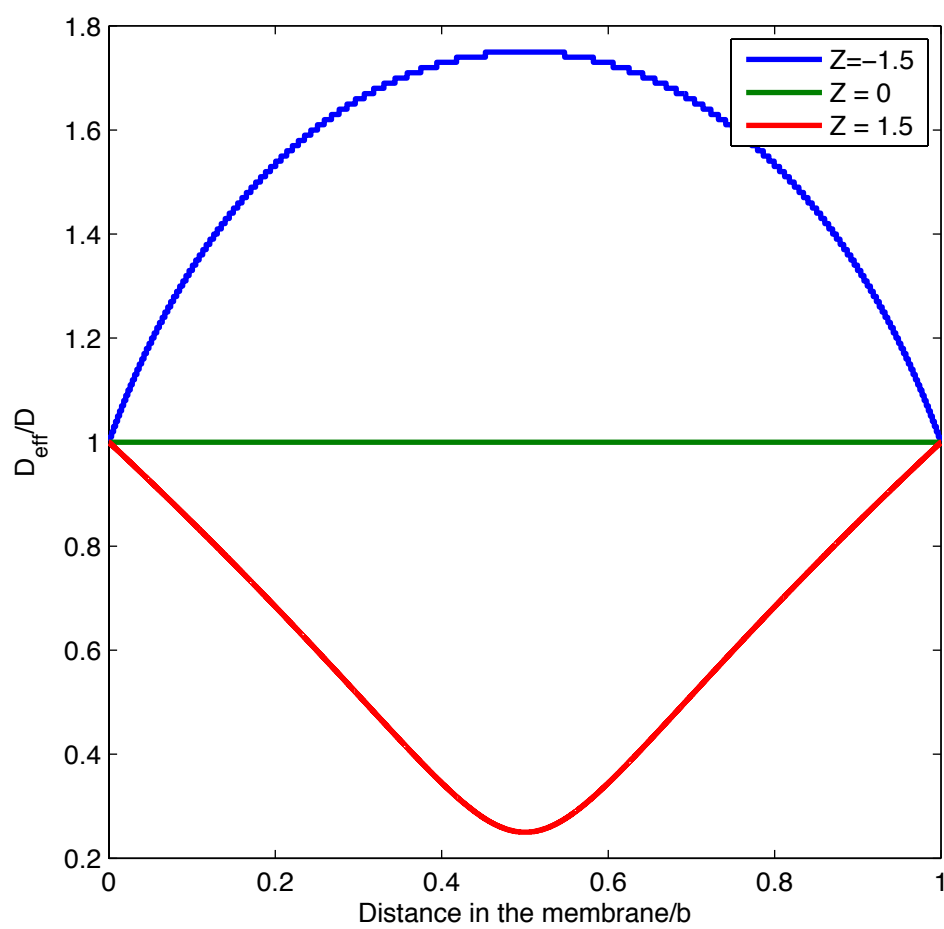


Figure 4e

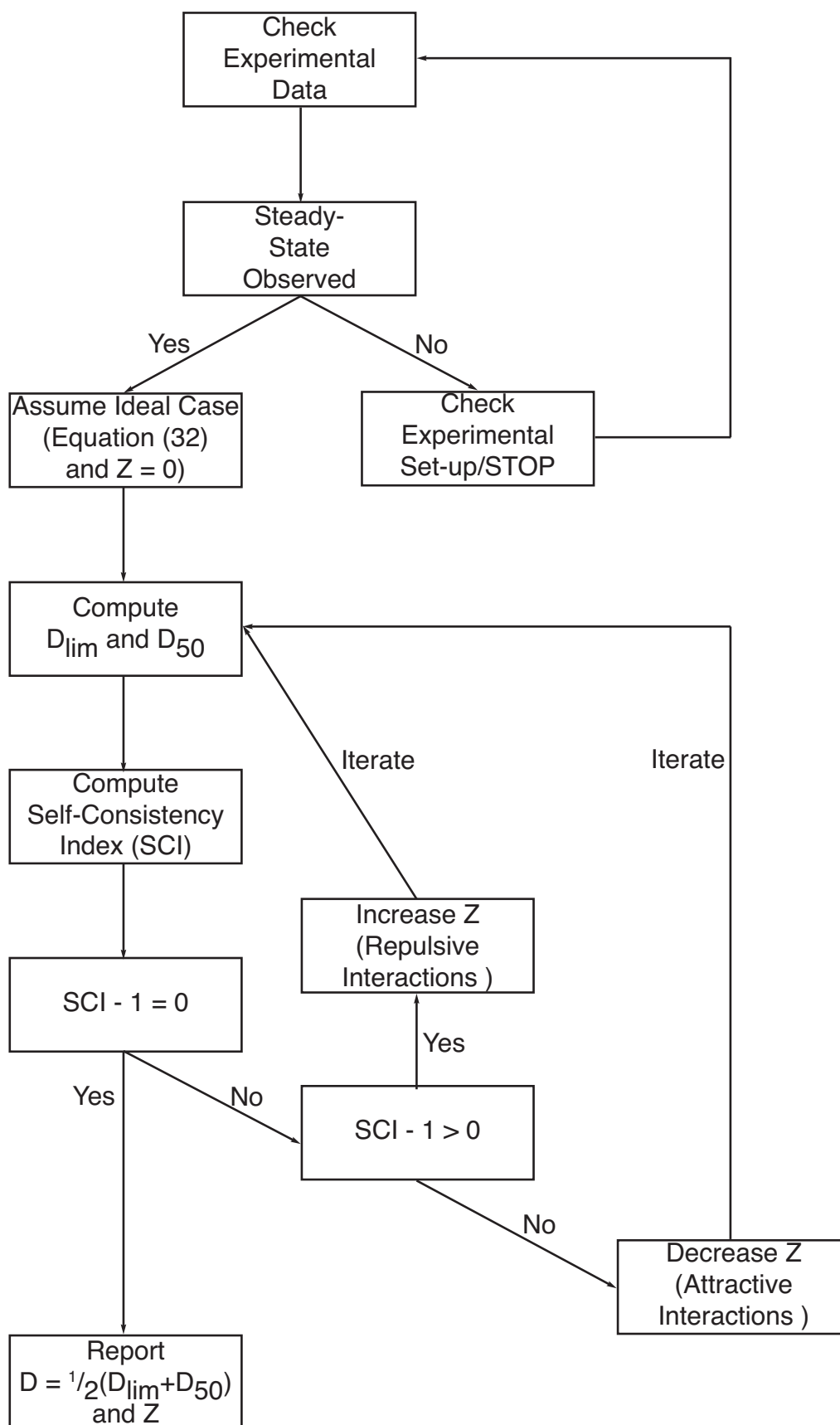


Figure 5a

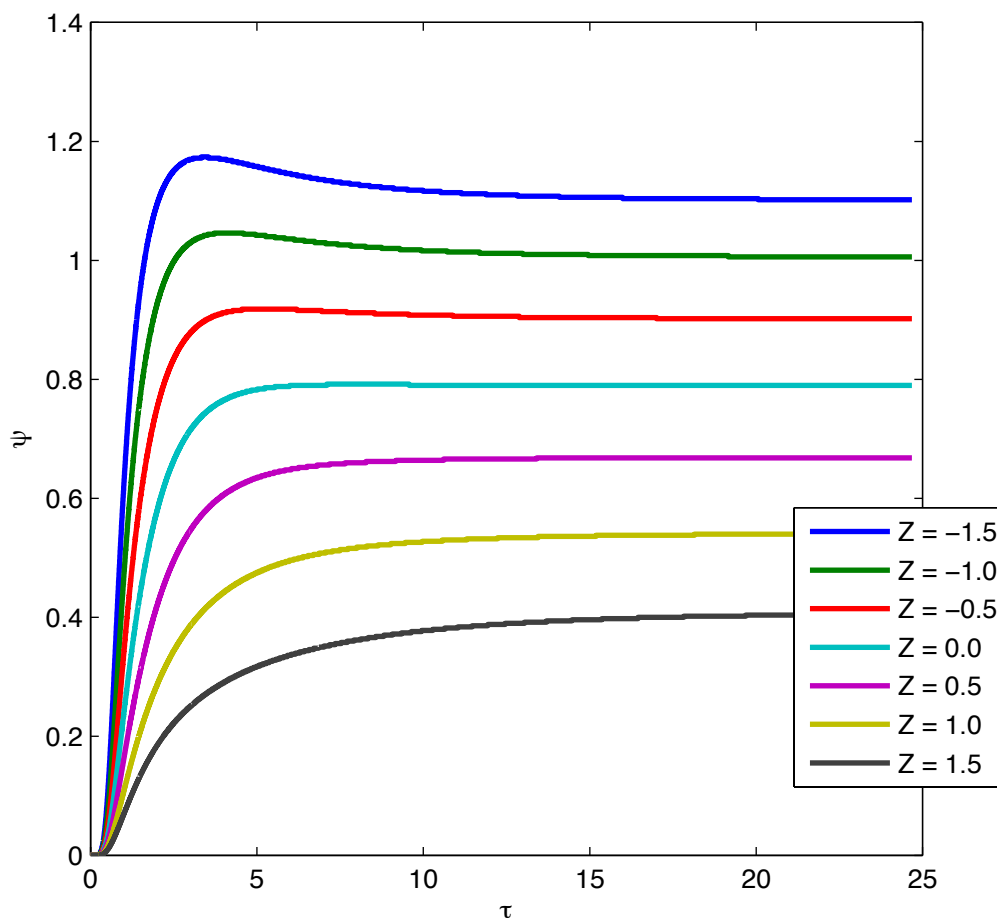


Figure 5b(i)

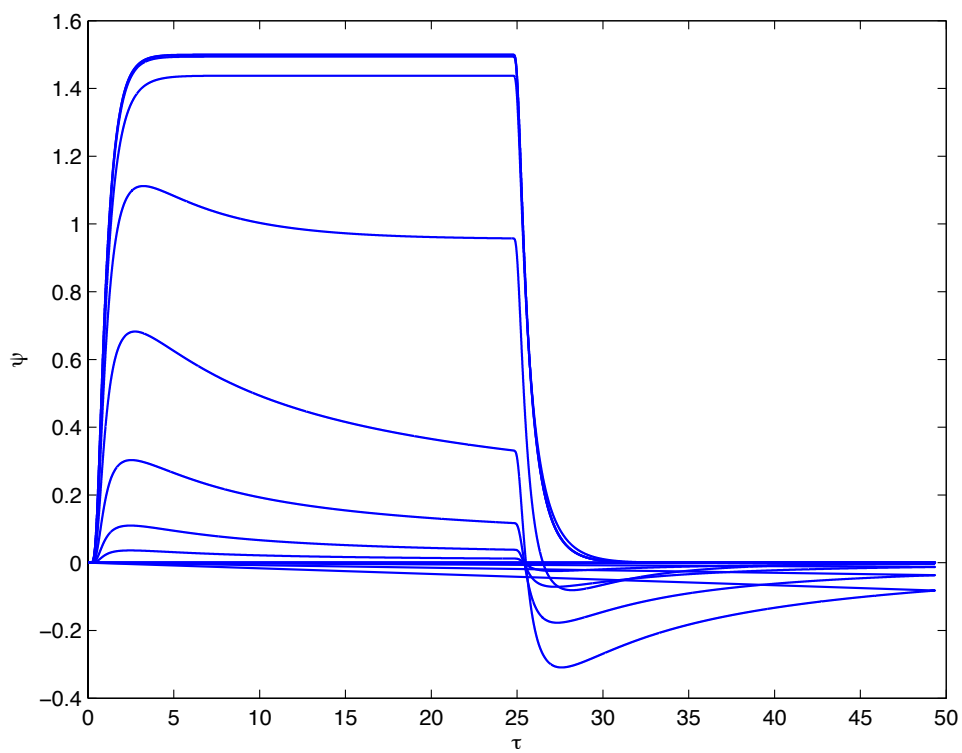


Figure 5b(ii)

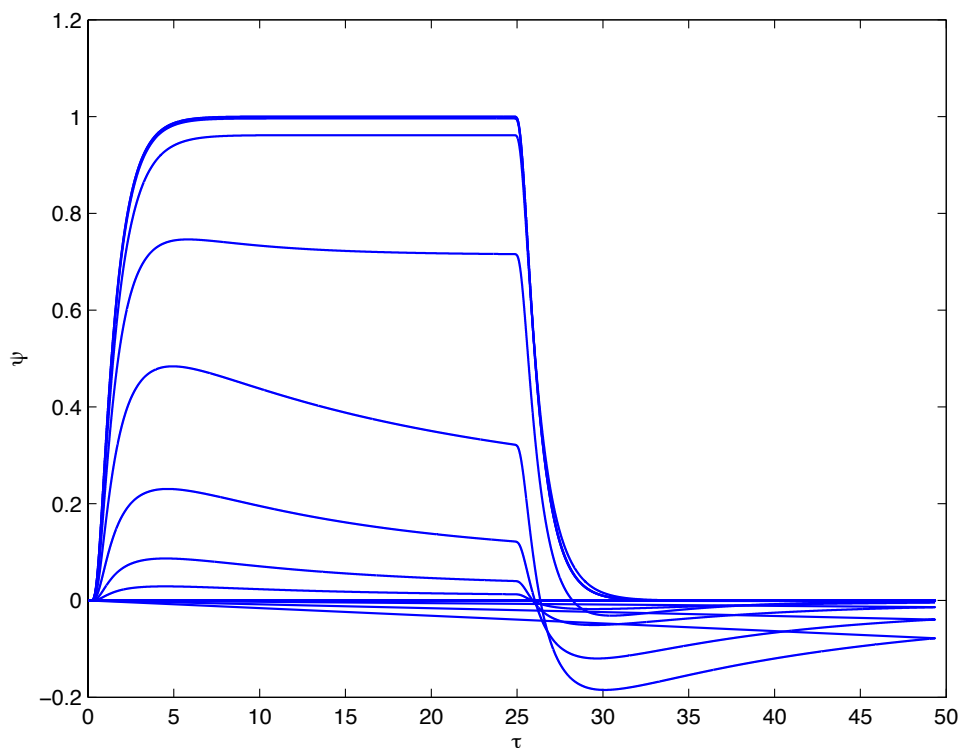


Figure 5b(iii)

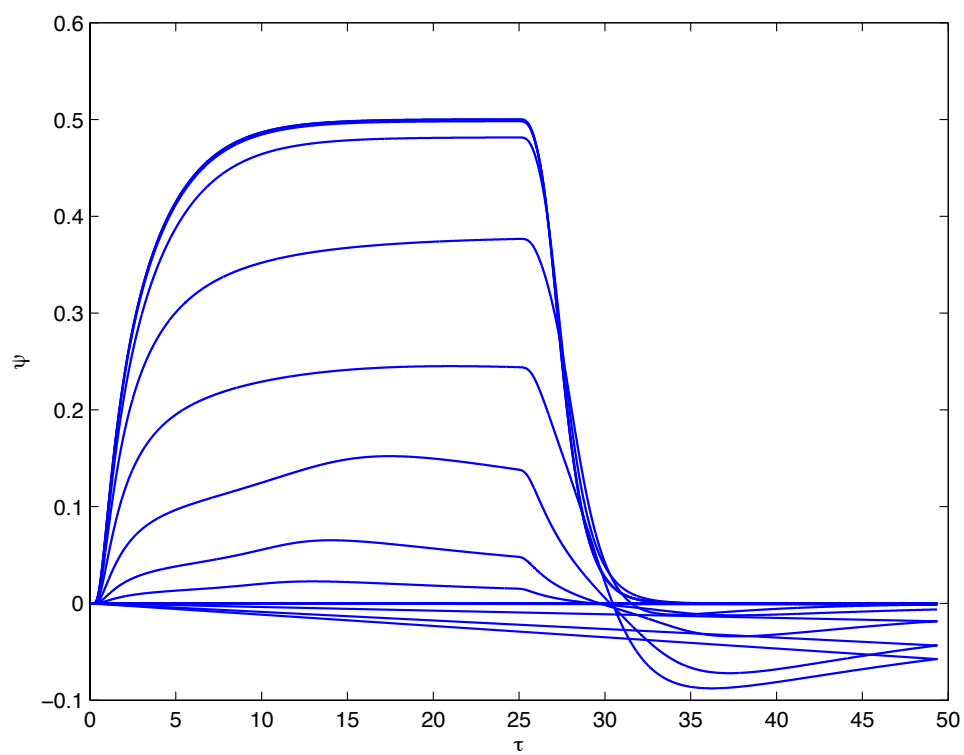


Figure 5c

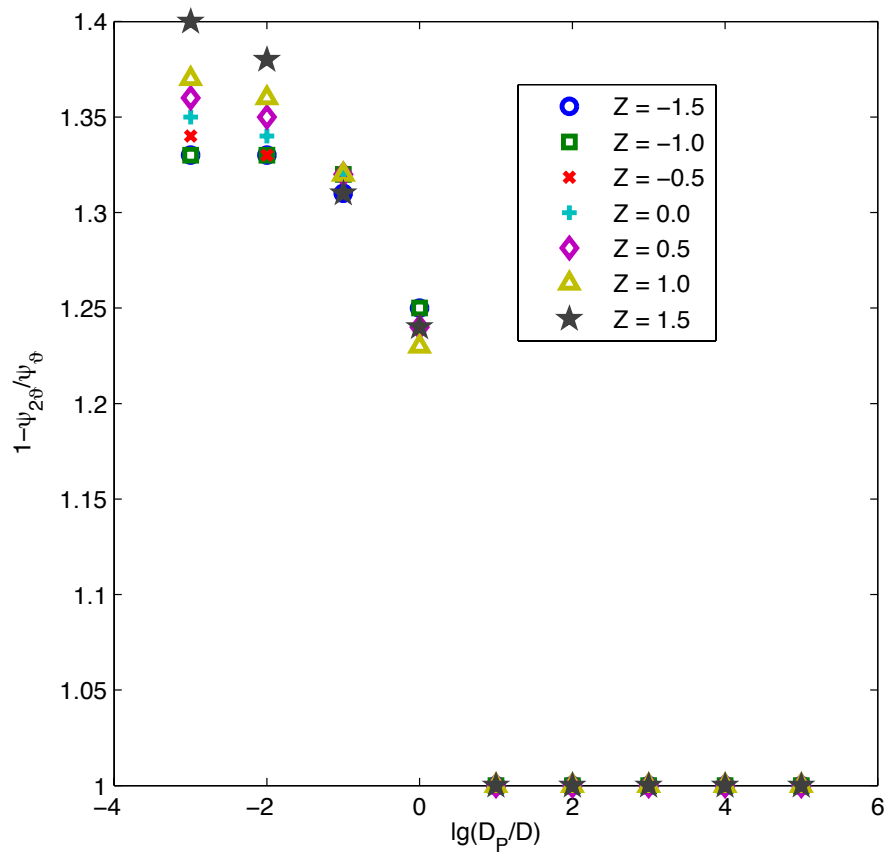


Figure 6a

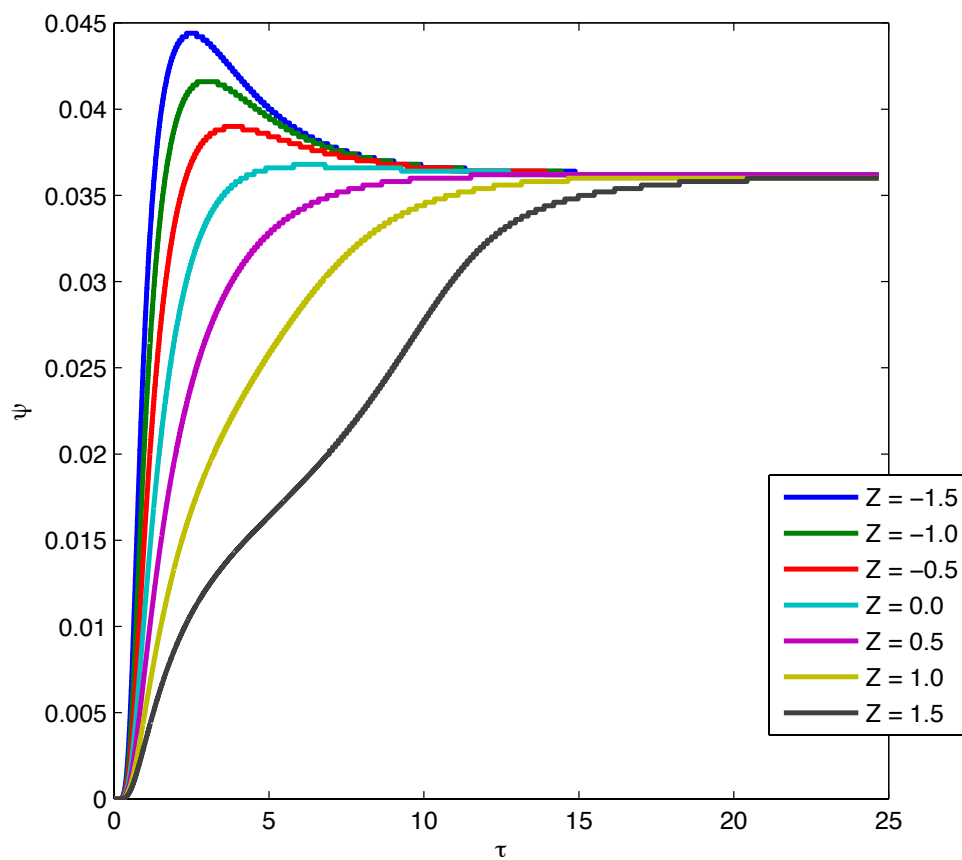


Figure 6b(i)

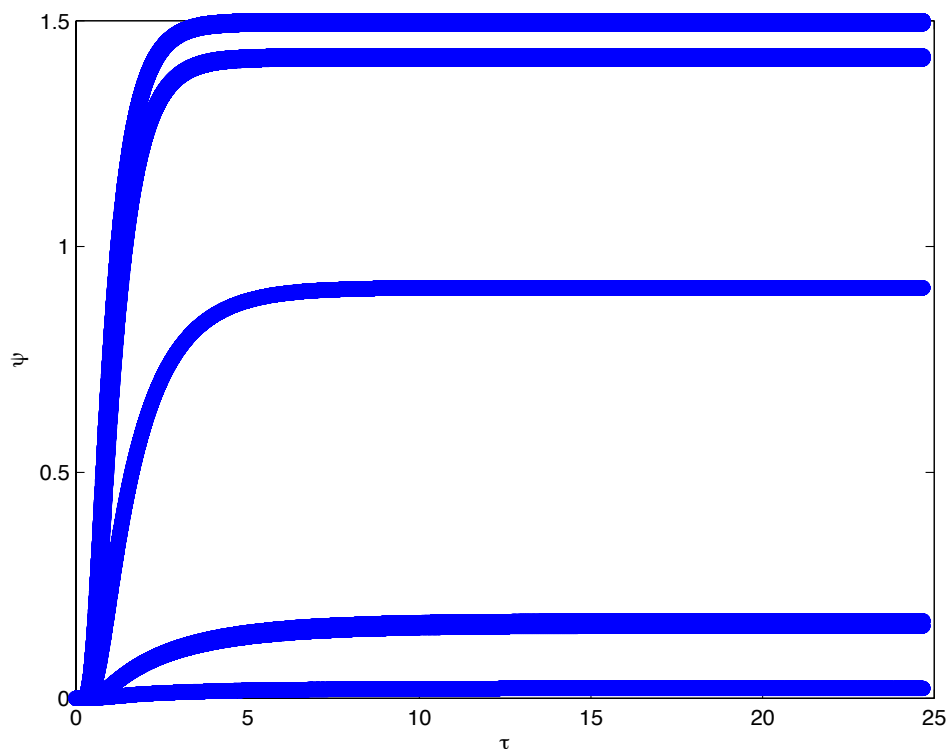


Figure 6b(ii)

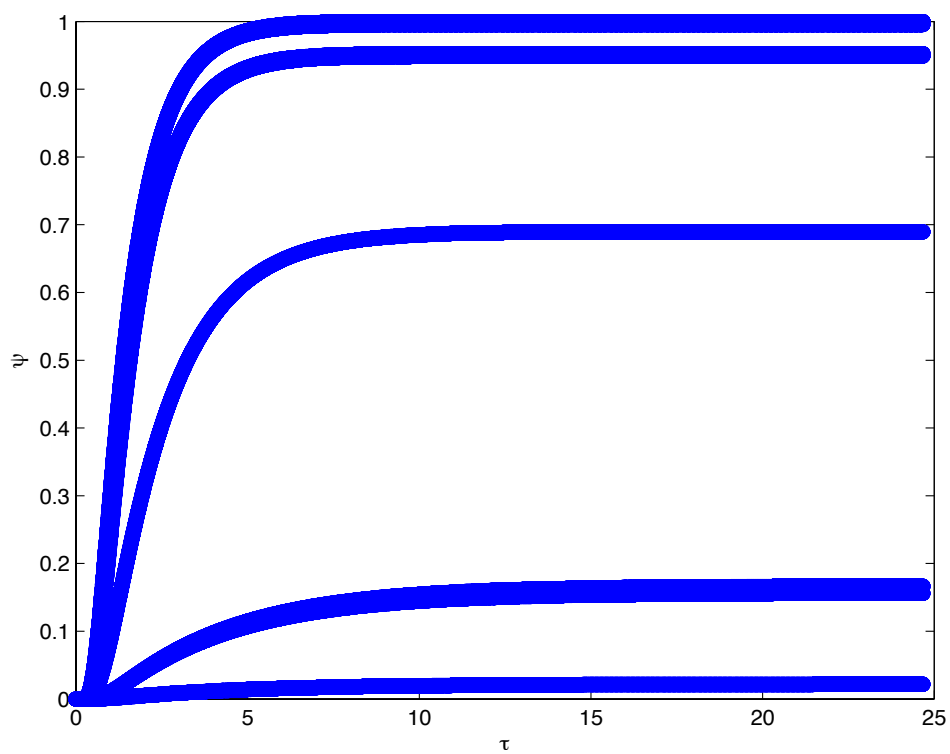


Figure 6b(iii)

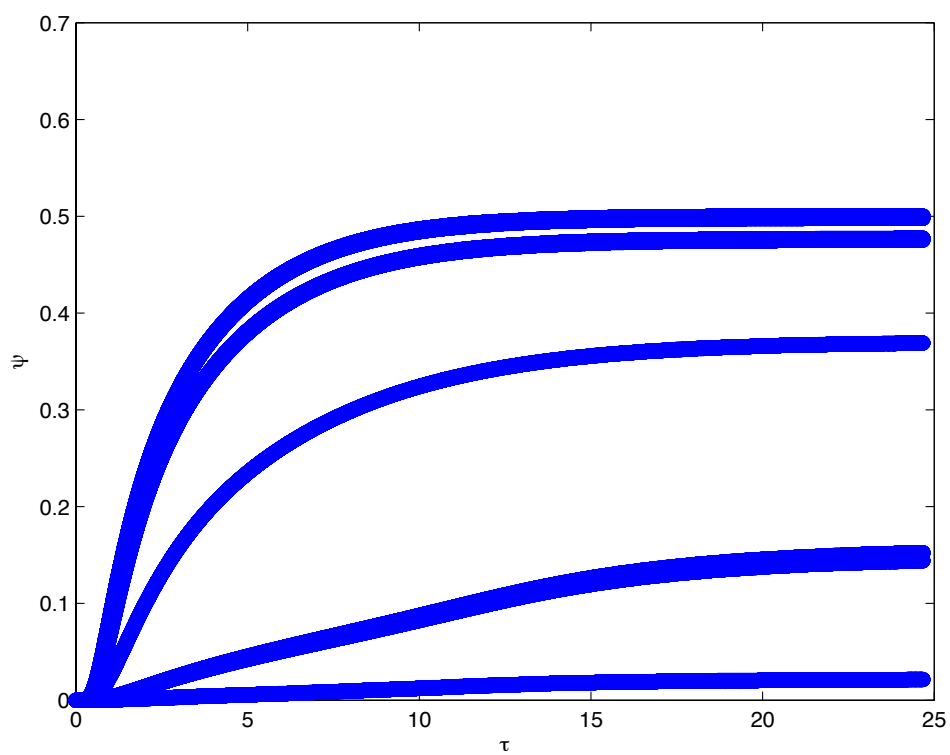
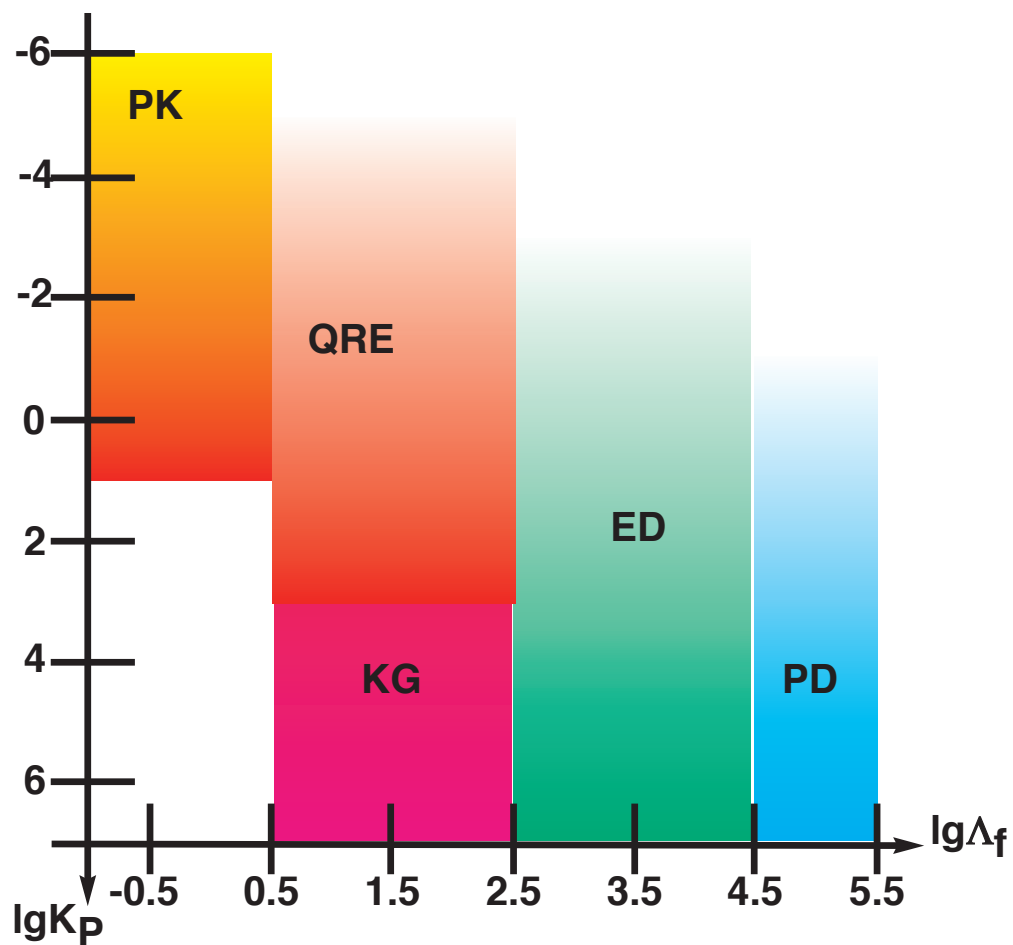


Figure 6c



1
2
3
4
5
6
7
8
9
10
11
12
13
14
15
16
17
18
19
20
21
22
23
24
25
26
27
28
29
30
31
32
33
34
35
36
37
38
39
40
41
42
43
44
45
46
47
48
49
50
51
52
53
54
55
56
57
58
59
60